bioRxiv preprint doi: https://doi.org/10.1101/2020.01.17.911016; this version posted January 18, 2020. The copyright holder for this preprint (which was not certified by peer review) is the author/funder. All rights reserved. No reuse allowed without permission.

Skd3 (human *CLPB*) is a potent mitochondrial protein disaggregase that is inactivated by 3-methylglutaconic aciduria-linked mutations

Ryan R. Cupo[1,2] and James Shorter[1,2*]

[1]Department of Biochemistry and Biophysics, [2]Pharmacology Graduate Group, Perelman School of Medicine at the University of Pennsylvania, Philadelphia, PA 19104, U.S.A.

*Correspondence: jshorter@pennmedicine.upenn.edu

bioRxiv preprint doi: https://doi.org/10.1101/2020.01.17.911016; this version posted January 18, 2020. The copyright holder for this preprint (which was not certified by peer review) is the author/funder. All rights reserved. No reuse allowed without permission.

ABSTRACT

Cells have evolved specialized protein disaggregases to reverse toxic protein aggregation and restore protein functionality. In nonmetazoan eukaryotes, the AAA+ disaggregase Hsp78 resolubilizes and reactivates proteins in mitochondria. Curiously, metazoa lack Hsp78. Hence, whether metazoan mitochondria reactivate aggregated proteins is unknown. Here, we establish that a mitochondrial AAA+ protein, Skd3 (human *CLPB*), couples ATP hydrolysis to protein disaggregation and reactivation. The Skd3 ankyrin-repeat domain combines with conserved AAA+ elements to enable stand-alone disaggregase activity. A mitochondrial inner-membrane protease, PARL, removes an autoinhibitory peptide from Skd3 to greatly enhance disaggregase activity. Indeed, PARL-activated Skd3 dissolves α-synuclein fibrils connected to Parkinson's disease. Human cells lacking Skd3 exhibit reduced solubility of various mitochondrial proteins, including anti-apoptotic Hax1. Importantly, Skd3 variants linked to 3-methylglutaconic aciduria, a severe mitochondrial disorder, display diminished disaggregase activity (but not always reduced ATPase activity), which predicts disease severity. Thus, Skd3 is a potent protein disaggregase critical for human health.

bioRxiv preprint doi: https://doi.org/10.1101/2020.01.17.911016; this version posted January 18, 2020. The copyright holder for this preprint (which was not certified by peer review) is the author/funder. All rights reserved. No reuse allowed without permission.

INTRODUCTION

Protein aggregation and aberrant phase transitions arise from a variety of cellular stressors and can be highly toxic (Chuang et al., 2018; Eisele et al., 2015; Guo et al., 2019). To counter this challenge, cells have evolved specialized protein disaggregases to reverse aggregation and restore resolubilized proteins to native structure and function (Shorter, 2017; Shorter and Southworth, 2019). Indeed, protein disaggregases are conserved across all domains of life, with orthologues of Hsp104, a ring-shaped hexameric AAA+ protein, powering protein disaggregation and reactivation (as opposed to degradation) in eubacteria and nonmetazoan eukaryotes (Glover and Lindquist, 1998; Goloubinoff et al., 1999; Queitsch et al., 2000; Shorter, 2008). In nonmetazoan eukaryotes, Hsp104 functions in the cytoplasm and nucleus (Parsell et al., 1994; Tkach and Glover, 2008; Wallace et al., 2015), whereas the closely-related AAA+ disaggregase, Hsp78, resolubilizes and reactivates proteins in mitochondria (Krzewska et al., 2001; Schmitt et al., 1996). Curiously, at the evolutionary transition from protozoa to metazoa both Hsp104 and Hsp78 are lost and are subsequently absent from all animal species (Erives and Fassler, 2015). This loss off Hsp104 and Hsp78 is perplexing given that toxic protein aggregation remains a major challenge in metazoa (Eisele et al., 2015). Indeed, it is even more baffling since ectopic expression of Hsp104 is well tolerated by animal cells and can be neuroprotective in animal models of neurodegenerative disease (Cushman-Nick et al., 2013; Dandoy-Dron et al., 2006; Jackrel et al., 2014; Lo Bianco et al., 2008; Perrin et al., 2007; Satyal et al., 2000; Vacher et al., 2005).

Metazoa may partially compensate for the absence of Hsp104 activity in the cytoplasm and nucleus with alternative general protein-disaggregase systems, such as Hsp110, Hsp70, Hsp40,

bioRxiv preprint doi: https://doi.org/10.1101/2020.01.17.911016; this version posted January 18, 2020. The copyright holder for this preprint (which was not certified by peer review) is the author/funder. All rights reserved. No reuse allowed without permission.

and small heat-shock proteins (Mattoo et al., 2013; Nillegoda et al., 2015; Shorter, 2011) as well as client-specific disaggregases in the cytoplasm such as nuclear-import receptors (Guo et al., 2019; Guo et al., 2018; Niaki et al., 2020; Yoshizawa et al., 2018). However, Hsp110 is not found in mitochondria (Voos and Rottgers, 2002). Thus, it continues to remain uncertain whether, in the absence of Hsp78, metazoan mitochondria harbor a disaggregase that solubilizes and reactivates aggregated proteins.

Here, we investigate if Skd3 (human *CLPB*) might act as a mitochondrial protein disaggregase in metazoa (Fig. 1a). Skd3 is a ubiquitously expressed, mitochondrial AAA+ protein of poorly-defined function, which is related to Hsp104 and Hsp78 via its HCLR clade AAA+ domain (Fig. 1a, S1) (Erzberger and Berger, 2006; Perier et al., 1995). Skd3 appears to play an important role in maintaining mitochondrial structure and function (Chen et al., 2019). Curiously, Skd3 first appears in evolution alongside Hsp104 and Hsp78 in choanoflagellates, a group of free-living unicellular and colonial flagellate eukaryotes that are the closest extant protozoan relatives of animals (Fig. 1b and S2) (Brunet and King, 2017; Erives and Fassler, 2015). During the complex evolutionary transition from protozoa to metazoa, Skd3 is retained, whereas Hsp104 and Hsp78 are lost (Erives and Fassler, 2015). Indeed, Skd3 is conserved in many metazoan lineages (Fig. 1a,b, S1, and S2) (Erives and Fassler, 2015).

Skd3 is comprised of a mitochondrial-targeting signal (MTS), followed by a short hydrophobic stretch, an ankyrin-repeat domain (ANK), an AAA+ nucleotide-binding domain (NBD), and a small C-terminal domain (CTD) (Fig. 1a). The Skd3 NBD closely resembles NBD2 of Hsp104 and Hsp78 (Fig. 1a, S1). Aside from this similarity, Skd3 is highly divergent from Hsp104 and

bioRxiv preprint doi: https://doi.org/10.1101/2020.01.17.911016; this version posted January 18, 2020. The copyright holder for this preprint (which was not certified by peer review) is the author/funder. All rights reserved. No reuse allowed without permission.

Hsp78 (Fig. 1a, S1). For example, Skd3, Hsp104, and Hsp78 all have short CTDs, but these are divergent with the Skd3 CTD being basic compared to the more acidic Hsp104 and Hsp78 CTDs (Fig. S1). Moreover, the other domains in Hsp104 (N-terminal domain [NTD], NBD1, and middle domain [MD]) and Hsp78 (NBD1 and MD) are not found in Skd3 (Fig. 1a, S1). In their place, is an ankyrin-repeat domain (Fig. 1a), which interestingly is an important substrate-binding domain of another protein disaggregase, chloroplast signal recognition particle 43 (cpSRP43) (Jaru-Ampornpan et al., 2013; Jaru-Ampornpan et al., 2010; McAvoy et al., 2018; Nguyen et al., 2013).

Importantly, mutations in the Skd3 ankyrin-repeat domain and NBD are linked to the rare, but severe mitochondrial disorder, 3-methylglutaconic aciduria, type VII (MGCA7) (Capo-Chichi et al., 2015; Kanabus et al., 2015; Kiykim et al., 2016; Pronicka et al., 2017; Saunders et al., 2015; Wortmann et al., 2016; Wortmann et al., 2015). MGCA7 is an autosomal recessive metabolic disorder that presents with increased levels of 3-methylglutaconic acid (3-MGA), neurologic deterioration, and neutropenia (Wortmann et al., 2016). Typically, patients present with infantile onset of a progressive encephalopathy with movement abnormalities and delayed psychomotor development (Wortmann et al., 2016). Other common, but variable, phenotypes include cataracts, seizures, and recurrent infections (Wortmann et al., 2016). These issues can be severe with afflicted infants typically only living for a few weeks or months (Wortmann et al., 2016). Patients may also present with more moderate phenotypes, including neutropenia, hypotonia, spasticity, movement abnormalities, epilepsy, and intellectual disability (Wortmann et al., 2016). Mildly affected individuals have no neurological problems, normal life expectancy, but present with neutropenia (Wortmann et al., 2016). There is no cure and no effective therapeutics for

bioRxiv preprint doi: https://doi.org/10.1101/2020.01.17.911016; this version posted January 18, 2020. The copyright holder for this preprint (which was not certified by peer review) is the author/funder. All rights reserved. No reuse allowed without permission.

severe or moderate forms of MGCA7. Moreover, little is known about how Skd3 mutations might cause disease.

Collectively, these various observations concerning Skd3 led us to hypothesize that Skd3 is a metazoan mitochondrial protein disaggregase of key importance for mitochondrial proteostasis. We further hypothesized that MGCA7-associated Skd3 mutations would disrupt disaggregase activity. Our investigation of these hypotheses is detailed below. Briefly, we find that Skd3 is an ATP-dependent mitochondrial protein disaggregase that is activated by the rhomboid protease PARL and inactivated by MGCA7-linked mutations.

bioRxiv preprint doi: https://doi.org/10.1101/2020.01.17.911016; this version posted January 18, 2020. The copyright holder for this preprint (which was not certified by peer review) is the author/funder. All rights reserved. No reuse allowed without permission.

RESULTS

Skd3 couples ATP hydrolysis to protein disaggregation and reactivation

To biochemically dissect the activity of Skd3, we purified full-length Skd3 (see Materials and methods), lacking the mitochondrial targeting signal, which is cleaved by the mitochondrial-processing peptidase (MPP) upon import into mitochondria (termed $_{MPP}$Skd3) (Fig. 2a, S3a-d) (Claros and Vincens, 1996; Wortmann et al., 2015). We first assessed that ATPase activity of $_{MPP}$Skd3 and found that it is active (Fig. 2b, S4a). Indeed, $_{MPP}$Skd3 displayed robust ATPase activity that was comparable to Hsp104 (Fig. 2b, S4a).

To determine if $_{MPP}$Skd3 is a disaggregase we used a classic aggregated substrate, urea-denatured firefly luciferase aggregates, which form aggregated structures of ~500–2,000 kDa and greater in size that are devoid of luciferase activity (DeSantis et al., 2012; Glover and Lindquist, 1998). $_{MPP}$Skd3 displayed robust disaggregase activity in the presence of ATP (Fig. 2c, S4b,c). Indeed, $_{MPP}$Skd3 displayed ~40% of the disaggregase activity of Hsp104 plus Hsp70 and Hsp40 under these conditions (Fig. 2c). While Hsp104 required the presence of Hsp70 and Hsp40 disaggregate luciferase (Fig. 2c, S4b,c) (DeSantis et al., 2012; Glover and Lindquist, 1998), $_{MPP}$Skd3 had no requirement for Hsp70 and Hsp40 (Fig. 2c, S4b,c). This finding indicates that $_{MPP}$Skd3 is a stand-alone disaggregase.

Next, we assessed the nucleotide requirements for $_{MPP}$Skd3 disaggregase activity. $_{MPP}$Skd3 disaggregase activity was supported by ATP but not by the absence of nucleotide or the presence of ADP (Fig. 2c, S4b, d). Likewise, neither the non-hydrolyzable ATP analogue, AMP-PNP, nor the slowly hydrolyzable ATP analogue, ATPγS, could support $_{MPP}$Skd3 disaggregase activity

bioRxiv preprint doi: https://doi.org/10.1101/2020.01.17.911016; this version posted January 18, 2020. The copyright holder for this preprint (which was not certified by peer review) is the author/funder. All rights reserved. No reuse allowed without permission.

(Fig. S4b, d). Collectively, these data suggest that $_{MPP}$Skd3 disaggregase activity requires multiple rounds of rapid ATP binding and hydrolysis, which is mechanistically similar to Hsp104 (Shorter and Lindquist, 2004, 2006).

We next investigated the role of conserved AAA+ elements in Skd3 activity. Thus, we mutated: (1) a critical lysine in the Walker A motif to alanine (K387A), which is predicted to disrupt ATP binding and hydrolysis (Hanson and Whiteheart, 2005); (2) a critical glutamate in the Walker B motif to glutamine (E455Q), which is predicted to disrupt ATP hydrolysis but not ATP binding (Hanson and Whiteheart, 2005); and (3) a highly-conserved tyrosine in the predicted -GYVG- substrate-binding loop to alanine that is predicted to disrupt substrate binding (Y430A) (Gates et al., 2017; Hanson and Whiteheart, 2005). The equivalent Walker A, Walker B, and substrate-binding loop mutations in NBD1 and NBD2 of Hsp104 severely disrupt disaggregase activity (DeSantis et al., 2012; Lum et al., 2004; Torrente et al., 2016). Likewise, $_{MPP}$Skd3^{K387A} (Walker A mutant) and $_{MPP}$Skd3^{E455Q} (Walker B mutant) displayed greatly reduced ATPase and disaggregase activity (Fig. 2d, e). Thus, $_{MPP}$Skd3 couples ATP binding and hydrolysis to protein disaggregation.

Interestingly, the pore-loop variant, $_{MPP}$Skd3^{Y430A}, exhibited reduced ATPase activity compared to $_{MPP}$Skd3, but much higher ATPase activity than $_{MPP}$Skd3^{K387A} and $_{MPP}$Skd3^{E455Q} (Fig. 2d). This reduction in ATPase activity was unexpected as equivalent mutations in Hsp104 do not affect ATPase activity (DeSantis et al., 2012; Lum et al., 2008; Lum et al., 2004; Torrente et al., 2016). $_{MPP}$Skd3^{Y430A} was also devoid of disaggregase activity (Fig. 2e). The inhibition of disaggregase activity by Y430A was much more severe than the inhibition of ATPase activity (Fig. 2d, e),

bioRxiv preprint doi: https://doi.org/10.1101/2020.01.17.911016; this version posted January 18, 2020. The copyright holder for this preprint (which was not certified by peer review) is the author/funder. All rights reserved. No reuse allowed without permission.

which suggests that the pore-loop Y430 might make direct contact with substrate to drive protein disaggregation as in Hsp104 (DeSantis et al., 2012; Gates et al., 2017). Thus, the conserved substrate-binding tyrosine of the -GYVG- pore-loop is critical for $_{MPP}$Skd3 disaggregase activity.

Skd3 disaggregase activity is enhanced by PARL cleavage

We noticed that Skd3 contains an undefined, 35-amino acid, hydrophobic stretch between the N-terminal MTS and the ankyrin-repeat domain (Fig. 1a, S5a). Intriguingly, Skd3 is cleaved by the inner-membrane rhomboid protease, PARL, at amino acid 127, between the 35-amino acid, hydrophobic stretch and the ankyrin-repeat domain (Fig. S5a) (Saita et al., 2017; Spinazzi et al., 2019). Sequence analysis shows that the Skd3 35-amino acid, hydrophobic stretch and the PARL-cleavage motif are both highly conserved among mammalian species (Fig. S6a). Thus, we hypothesized that this 35-amino acid, hydrophobic stretch might be auto-inhibitory for Skd3 activity.

To determine whether PARL cleavage of this 35-amino acid, hydrophobic stretch regulates Skd3 activity, we purified Skd3 without this region ($_{PARL}$Skd3) (Fig. 3a). We found that PARL cleavage slightly decreased Skd3 ATPase activity compared to $_{MPP}$Skd3 (Fig. 3b, S6b). Moreover, we find that $_{MPP}$Skd3 ATPase activity is not stimulated by the model substrate, casein, a classic peptide-stimulator of Hsp104 ATPase activity (Fig. S7a) (Cashikar et al., 2002; Gates et al., 2017). By contrast, $_{PARL}$Skd3 ATPase activity is mildly stimulated by casein (Fig. S7a). This finding indicates that $_{PARL}$Skd3 may interact more effectively with substrates than $_{MPP}$Skd3 due to the removal of the 35-amino acid, hydrophobic stretch.

bioRxiv preprint doi: https://doi.org/10.1101/2020.01.17.911016; this version posted January 18, 2020. The copyright holder for this preprint (which was not certified by peer review) is the author/funder. All rights reserved. No reuse allowed without permission.

Remarkably, PARL cleavage unleashes Skd3 disaggregase activity (Fig. 3c, S6c,d). Indeed, $_{PARL}$Skd3 exhibited over 10-fold higher disaggregase activity compared to $_{MPP}$Skd3 and over five-fold higher disaggregation activity than Hsp104 plus Hsp70 and Hsp40, despite $_{PARL}$Skd3 having lower ATPase activity when compared to $_{MPP}$Skd3 (Fig. 3b,c, S6b,c,d). These results demonstrate that Skd3 disaggregase activity is regulated by PARL and that PARL-activated Skd3 is a powerful, stand-alone protein disaggregase with comparable activity to potentiated Hsp104 variants (Jackrel et al., 2014; Jackrel and Shorter, 2014; Jackrel et al., 2015; Tariq et al., 2019; Tariq et al., 2018).

As with $_{MPP}$Skd3, we found that $_{PARL}$Skd3 disaggregase activity was supported by ATP, but not in the absence of nucleotide or in the presence of ADP, non-hydrolyzable AMP-PNP, or slowly hydrolyzable ATPγS (Fig. Fig. 3c, S6e). Likewise, $_{PARL}$Skd3^{K387A} (Walker A mutant) and $_{PARL}$Skd3^{E455Q} (Walker B mutant) lacked ATPase and disaggregase activity (Fig. 3d, e), indicating that $_{PARL}$Skd3 couples ATP binding and hydrolysis to protein disaggregation. Curiously, $_{PARL}$Skd3^{Y430A} (pore-loop mutant) exhibited a larger reduction in ATPase activity than $_{MPP}$Skd3^{Y430A} (Fig. 2d, 3d), indicating that the conserved tyrosine in the conserved substrate-binding -GYVG- pore loop impacts ATPase activity in Skd3, whereas it has no effect in Hsp104 (DeSantis et al., 2012; Torrente et al., 2016). $_{PARL}$Skd3^{Y430A} was devoid of disaggregase activity (Fig. 3e), which could be due to reduced ATPase activity, reduced substrate binding, or both.

PARL-activated Skd3 dissolves α-synuclein fibrils

Next, we assessed whether $_{PARL}$Skd3 could disassemble a stable amyloid substrate, which makes more stringent demands on a disaggregase (DeSantis et al., 2012). Thus, we turned to α-

bioRxiv preprint doi: https://doi.org/10.1101/2020.01.17.911016; this version posted January 18, 2020. The copyright holder for this preprint (which was not certified by peer review) is the author/funder. All rights reserved. No reuse allowed without permission.

synuclein fibrils, which are connected to Parkinson's disease and various synucleinopathies (Henderson et al., 2019). We utilized a strain of synthetic α-synuclein fibrils capable of eliciting Parkinson's disease-like symptoms in mice (Luk et al., 2012). Using a sedimentation assay combined with a dot-blot, we found that $_{PARL}$Skd3 disaggregated these disease-causing fibrils in the presence, but not absence of ATP (Fig. 4a, b). Thus, $_{PARL}$Skd3 is a powerful protein disaggregase, which could be harnessed as a therapeutic agent to eliminate disease-causing α-synuclein fibrils that underlie Parkinson's disease and other synucleinopathies.

Skd3 disaggregase activity requires the ankyrin-repeat domain and NBD

To further investigate the mechanism of Skd3 disaggregase activity, we purified the isolated ankyrin-repeat domain and NBD as separate proteins (Fig. 5a). Neither the isolated ankyrin-repeat domain nor the isolated NBD exhibited ATPase activity or disaggregase activity (Fig. 5b, c). The lack of ATPase activity and disaggregase activity of the isolated NBD is consistent with a similar lack of activity of isolated NBD2 from Hsp104 or bacterial ClpB (Beinker et al., 2005; Hattendorf and Lindquist, 2002; Mogk et al., 2003). Thus, the ankyrin-repeat domain and NBD combine in cis to enable Skd3 ATPase activity and disaggregase activity. We also tested whether the two domains could combine in trans as two separate proteins to yield an ATPase or disaggregase. However, we found that equimolar amounts of the ankyrin-repeat domain and NBD were also inactive (Fig. 5b, c). Thus, Skd3 is unlike bacterial ClpB, which can be reconstituted in trans by separate NTD-NBD1-MD and NBD2 proteins (Beinker et al., 2005). These findings suggest that the covalent linkage of the ankyrin-repeat domain and NBD is critical for forming a functional ATPase and disaggregase. Importantly, these findings predict that truncated MGCA7-linked Skd3 variants, such as R250* and K321* (where * indicates a stop

bioRxiv preprint doi: https://doi.org/10.1101/2020.01.17.911016; this version posted January 18, 2020. The copyright holder for this preprint (which was not certified by peer review) is the author/funder. All rights reserved. No reuse allowed without permission.

codon), which lack the NBD would be inactive for protein disaggregation and indeed any ATPase-dependent activities.

Skd3 disaggregase activity is not stimulated by Hsp70 and Hsp40

Hsp104 and Hsp78 collaborate with Hsp70 and Hsp40 to disaggregate many substrates (DeSantis et al., 2012; Glover and Lindquist, 1998; Krzewska et al., 2001). By contrast, Skd3 does not require Hsp70 and Hsp40 for protein disaggregation (Fig. 2b, e, 3c, e, 4a, b). This finding is consistent with Skd3 lacking the NTD, NBD1, and MD of Hsp104, which interact with Hsp70 (DeSantis et al., 2014; Lee et al., 2013; Sweeny et al., 2015; Sweeny et al., 2019). Nonetheless, Hsp70 and Hsp40 might still augment Skd3 disaggregase activity. Thus, we tested if Hsp70 and Hsp40 could stimulate Skd3 disaggregase activity. However, neither $_{MPP}$Skd3 nor $_{PARL}$Skd3, disaggregase activity was stimulated by Hsp70 and Hsp40 (Fig. 6a, b). Thus, Skd3 is a stand-alone disaggregase that works independently of the Hsp70 chaperone system.

Human cells lacking Skd3 exhibit reduced solubility of mitochondrial proteins

Given the potent disaggregase activity of Skd3, we predicted that deletion of Skd3 in human cells would result in decreased protein solubility in mitochondria. To determine the effect of Skd3 on protein solubility in mitochondria, we compared the relative solubility of the mitochondrial proteome in wild-type and Skd3 knockout human HAP1 cells (Fig. S8a) using mass spectrometry as described in Fig. 7a. Overall, we observed decreased protein solubility in mitochondria from the Skd3 knockout cells when compared to their wild-type counterparts (Fig. 7b, S9a). Using Gene Ontology (GO) analysis for cellular component, we found that proteins in the inner mitochondrial membrane and intermembrane space were enriched in the insoluble

bioRxiv preprint doi: https://doi.org/10.1101/2020.01.17.911016; this version posted January 18, 2020. The copyright holder for this preprint (which was not certified by peer review) is the author/funder. All rights reserved. No reuse allowed without permission.

fraction in the absence of Skd3 (Fig. S9a) (Ashburner et al., 2000; Mi et al., 2019; The Gene Ontology, 2019). Using GO analysis for biological process, we found that proteins involved in calcium import into mitochondria, chaperone-mediated protein transport, protein insertion into the mitochondrial inner membrane, mitochondrial electron transport, mitochondrial respiratory-chain complex assembly, and cellular response to hypoxia are more insoluble in Skd3 knockout cells compared to wild-type cells (Fig. 7c, S9b) (Ashburner et al., 2000; Mi et al., 2019; The Gene Ontology, 2019).

Specifically, we find that HAX1, OPA1, PARL, SMAC/DIABLO, and HTRA2 are more insoluble, which implicates a key role for Skd3 in regulating apoptotic and proteolytic pathways (Baumann et al., 2014; Chai et al., 2000; Chao et al., 2008; Cipolat et al., 2006; Frezza et al., 2006; Klein et al., 2007; Saita et al., 2017). Additionally, the regulators of the mitochondrial calcium uniporter (MCU), MICU1 and MICU2 were found to be more insoluble in the knockout compared to the wild type, implicating Skd3 in the regulation of mitochondrial calcium transport (Csordas et al., 2013; Patron et al., 2014; Perocchi et al., 2010; Plovanich et al., 2013). We also observed an enrichment of translocase of the inner membrane (TIM) components, TIMM8A, TIMM8B, TIMM13, TIMM21, TIMM22, TIMM23, and TIMM50 in the insoluble fraction of Skd3 knockouts (Chacinska et al., 2005; Donzeau et al., 2000; Geissler et al., 2002; Meinecke et al., 2006; Mokranjac et al., 2003; Paschen et al., 2000; Sirrenberg et al., 1996; Yamamoto et al., 2002). Finally, we observed an enrichment in respiratory complex I and III proteins and their assembly factors such as NDUFA8, NDUFA11, NDUFA13, NDUFB7, NDUFB10, TTC19, COX11, and CYC1 (Fig. 6b and Table S1) (Angebault et al., 2015; Ghezzi et al., 2011; Spinazzi et al., 2019; Szklarczyk et al., 2011; Tzagoloff et al., 1990). Overall, these results suggest the

bioRxiv preprint doi: https://doi.org/10.1101/2020.01.17.911016; this version posted January 18, 2020. The copyright holder for this preprint (which was not certified by peer review) is the author/funder. All rights reserved. No reuse allowed without permission.

importance of Skd3 in maintaining the solubility of proteins of the inner mitochondrial membrane and intermembrane space, including key regulators in apoptosis, mitochondrial calcium regulation, protein import, and respiration. Thus, in cells Skd3 appears critical for protein solubility in the intermembrane space and mitochondrial inner membrane.

Skd3 promotes HAX1 solubility in human cells

HAX1 is a highly-disordered protein that has been previously identified as a Skd3 substrate both in cells and *in silico* (Fig. S10a) (Chen et al., 2019; Wortmann et al., 2015). HAX1 is an anti-apoptotic BCL-2 family protein that enables efficient cleavage of HTRA2 by PARL to promote cell survival (Chao et al., 2008; Klein et al., 2007). To test if Skd3 regulates HAX1 solubility in human cells, we compared the solubility of HAX1 in wild-type and Skd3-knockout HAP1 cells via sedimentation analysis and western blot. In wild-type cells, HAX1 remained predominantly soluble (Fig. 7d,e). However, when Skd3 was deleted HAX1 became predominantly insoluble (Fig. 7d,e). Thus, Skd3 is essential for HAX1 solubility in cells. Curiously, loss of Skd3 has been previously shown to promote apoptosis in specific contexts (Chen et al., 2019). Furthermore, HAX1 stability has been implicated as a regulator of apoptotic signaling (Baumann et al., 2014). Our data support a model whereby Skd3 exerts its anti-apoptotic effect by maintaining HAX1 solubility and contingent functionality.

MGCA7-linked Skd3 variants display diminished disaggregase activity

Skd3 has been implicated in a severe mitochondrial disorder, MGCA7, yet little is known about its contribution or function in this disease (Capo-Chichi et al., 2015; Kanabus et al., 2015; Kiykim et al., 2016; Pronicka et al., 2017; Saunders et al., 2015; Wortmann et al., 2016;

bioRxiv preprint doi: https://doi.org/10.1101/2020.01.17.911016; this version posted January 18, 2020. The copyright holder for this preprint (which was not certified by peer review) is the author/funder. All rights reserved. No reuse allowed without permission.

Wortmann et al., 2015). Indeed, many mutations in Skd3 are connected with MGCA7 (Fig. 8a). Most of these are clustered in the NBD, but several are also in the ankyrin-repeat domain, and one frameshift is found in the mitochondrial targeting signal (Fig. 8a). Some MGCA7-linked Skd3 variants, such as R250* and K321* (where * indicates a stop codon), lack the NBD and would be predicted in light of our findings to be incapable protein disaggregation and indeed any ATPase-dependent activities (Fig. 5b, c). We hypothesized that MGCA7-linked missense mutations also directly affect Skd3 disaggregase activity. To test this hypothesis, we purified MGCA7-linked variants of Skd3 from cases where both patient alleles bear the mutation, specifically: T268M, R475Q, A591V, and R650P (Pronicka et al., 2017). These Skd3 variants cause MGCA7 on a spectrum of clinical severity (Pronicka et al., 2017). The ankyrin-repeat variant, T268M, is linked to moderate MGCA7, whereas the NBD variants (R475Q, A591V, and R650P) are linked to severe MGCA7 (Pronicka et al., 2017).

Surprisingly, the ATPase activity varied for each MGCA7-linked variant. T268M had significantly increased ATPase activity, R475Q and A591V had marked decreased ATPase activity, and R650P ATPase was indistinguishable from wild type (Fig. 8b). These ATPase activities did not correlate with clinical severity (Fig. 8d) (Pronicka et al., 2017). Thus, Skd3 variant ATPase activity does not accurately predict MGCA7 severity, as the mutation associated with mild MGCA7 had elevated ATPase relative to wild type, whereas different mutations capable of causing severe MGCA7 could exhibit impaired or nearly wild-type ATPase activity

To address the disconnect between ATPase activity and MGCA7 disease severity, we next tested the disaggregase activity of these MGCA7-linked variants. Strikingly, and in contrast to ATPase

bioRxiv preprint doi: https://doi.org/10.1101/2020.01.17.911016; this version posted January 18, 2020. The copyright holder for this preprint (which was not certified by peer review) is the author/funder. All rights reserved. No reuse allowed without permission.

activity, we found disaggregase activity tracks closely with disease severity. T268M, the only moderate phenotype variant tested, had ~27% disaggregase activity compared to wild type. By contrast, the three severe MGCA7 variants, R475Q, A591V, and R650P abolish or diminish disaggregation activity with 0%, 0%, and ~4% disaggregation activity compared to wild type, respectively (Fig. 8c). Thus, disaggregase activity but not ATPase activity, is tightly correlated with clinical severity of MGCA7-linked mutations (Fig. 8d) (Pronicka et al., 2017). Taken together, our findings suggest that defects in Skd3 protein-disaggregase activity (and not other ATPase-related functions) are the driving factor in MGCA7 and pivotal to human health.

bioRxiv preprint doi: https://doi.org/10.1101/2020.01.17.911016; this version posted January 18, 2020. The copyright holder for this preprint (which was not certified by peer review) is the author/funder. All rights reserved. No reuse allowed without permission.

DISCUSSION

At the evolutionary transition from protozoa to metazoa, the potent mitochondrial AAA+ protein disaggregase, Hsp78, was lost. Thus, it has long remained unknown whether metazoan mitochondria disaggregate and reactivate aggregated proteins. Here, we establish that another AAA+ protein, Skd3, is a potent metazoan mitochondrial protein disaggregase. Skd3 is activated by a mitochondrial inner-membrane rhomboid protease, PARL (Fig. 9). PARL removes a hydrophobic auto-inhibitory sequence from the N-terminal region of Skd3, which prior to cleavage may limit Skd3 interactions with substrate (Fig. 9). In this way, Skd3 only becomes fully activated as a disaggregase once it reaches its final cellular destination.

Skd3 couples ATP binding and hydrolysis to protein disaggregation. To do so, Skd3 utilizes conserved AAA+ motifs in its NBD, including the Walker A and B motifs to bind and hydrolyze ATP, as well as a conserved pore-loop tyrosine, which likely engages substrate directly. However, the isolated NBD is insufficient for disaggregase activity, which indicates an important role for the ankyrin-repeat domain. Intriguingly, an ankyrin-repeat domain is also important for the activity of an unrelated ATP-independent protein disaggregase, cpSRP43, where it makes critical contacts with substrate (Jaru-Ampornpan et al., 2013; Jaru-Ampornpan et al., 2010; McAvoy et al., 2018; Nguyen et al., 2013). Thus, ankyrin-repeat domains appear to be a recurring feature of diverse protein disaggregases.

Importantly, Skd3 is a stand-alone disaggregase and does not require Hsp70 and Hsp40 for maximal activity. This finding is consistent with the absence of Hsp70-interacting domains (NTD, NBD1, and MD) found in Hsp104, which enable collaboration with Hsp70 (DeSantis et

bioRxiv preprint doi: https://doi.org/10.1101/2020.01.17.911016; this version posted January 18, 2020. The copyright holder for this preprint (which was not certified by peer review) is the author/funder. All rights reserved. No reuse allowed without permission.

al., 2014; Lee et al., 2013; Sweeny et al., 2015; Sweeny et al., 2019). Future structural and biochemical studies will further inform our mechanistic understanding of Skd3 disaggregase activity.

We establish that Skd3 can disaggregate disease-causing α-synuclein fibrils *in vitro*, demonstrating its robust activity as a disaggregase and identifying it as a novel target for synucleinopathies. The realization that human cells harbor a AAA+ protein disaggregase of greater potency than Hsp104 opens several therapeutic opportunities. Indeed, Skd3 is expressed in neurons and shifting localization of activated Skd3 to the cytoplasm could help combat cytoplasmic aggregates. Likewise, the expression of the $_{\text{PARL}}$Skd3 enhanced variant in the cytoplasm of dopaminergic neurons may elicit therapeutic benefit similar to Hsp104 and engineered variants in Parkinson's disease models (Jackrel et al., 2014; Lo Bianco et al., 2008; Tariq et al., 2019). Future studies will further inform our understanding of how to harness Skd3 disaggregase activity therapeutically in synucleinopathies such as Parkinson's disease and other neurodegenerative diseases connected with aberrant protein aggregation.

We demonstrate that Skd3 is essential for maintaining the solubility of mitochondrial inner-membrane and intermembrane space protein complexes and specifically disaggregates the anti-apoptotic protein HAX1 in human cells (Fig. 9). We suggest that HAX1 solubility is important for its anti-apoptotic effect. The precise mechanism of regulation between Skd3 and HAX1, PARL, OPA1, HTRA2, and SMAC/DIABLO warrants future study (Fig. 9).

bioRxiv preprint doi: https://doi.org/10.1101/2020.01.17.911016; this version posted January 18, 2020. The copyright holder for this preprint (which was not certified by peer review) is the author/funder. All rights reserved. No reuse allowed without permission.

In addition to finding that many human mitochondrial proteins are more insoluble in the absence of Skd3, a small fraction of proteins are more insoluble in the presence of Skd3. Closer analysis of these enriched proteins suggest many are mitochondrial matrix-associated, especially mitoribosome proteins (Fig. 7b, Table S2). The mitoribosome is a large, megadalton, sized protein complex that is much more proteinaceous than its cytoplasmic counterpart and assembles into larger polysomes during active translation (Couvillion et al., 2016; Greber and Ban, 2016; Saurer et al., 2019). Thus, changes in solubility of the mitoribosome components could be due to increased mitoribosome or polysome assembly in the presence of Skd3.

It is surprising that Skd3 solubilizes proteins of the mitochondrial intermembrane space and inner membrane, as Hsp78 is found in the mitochondrial matrix (Bateman et al., 2002; Germaniuk et al., 2002; Moczko et al., 1995; Rottgers et al., 2002; Schmitt et al., 1995; von Janowsky et al., 2006). Since Skd3 appears in evolution alongside Hsp78 in choanoflagellates it may have initially arisen to serve a subtly distinct function. We hypothesize that the increasing number and complexity of mitochondrial inner membrane protein assemblies (such as MICU1/MICU2/MCU and respiratory complex I) in choanoflagellates and metazoa might necessitate the requirement of Skd3 activity in the inner mitochondrial membrane and intermembrane space to maintain proteostasis in these compartments.

Mutations in Skd3 are connected to MGCA7, which can be a devastating disorder connected with severe neurologic deterioration, neutropenia, and death in infants (Wortmann et al., 2016). Importantly, we establish that diverse MGCA7-linked mutations in Skd3 impair disaggregase activity, but not necessarily ATPase activity (Fig. 9). The degree of impaired disaggregase

bioRxiv preprint doi: https://doi.org/10.1101/2020.01.17.911016; this version posted January 18, 2020. The copyright holder for this preprint (which was not certified by peer review) is the author/funder. All rights reserved. No reuse allowed without permission.

activity predicts the clinical severity of the disease, which suggests that disaggregase activity is a critical factor in disease. However, it is yet unclear which Skd3 substrate or substrates contribute to the MGCA7 etiology. Our mass-spectrometry data suggest that MGCA7 arises due to severely compromised proteostasis in the mitochondrial inner-membrane and intermembrane space (Fig. 9). Hence, small-molecule drugs that restore wild-type levels of disaggregase activity to MGCA7-linked Skd3 variants could be valuable therapeutics.

Finally, Skd3 has also emerged as a factor in Venetoclax resistance, a FDA-approved drug for the treatment of acute myeloid leukemia (AML), which exerts its mechanism via BCL-2 inhibition (Chen et al., 2019). These studies suggest that inhibition of Skd3 may be of critical therapeutic importance for treating Venetoclax-resistant cancers (Chen et al., 2019). Small-molecule screens targeted at finding inhibitors of Skd3 disaggregase activity may yield important drugs for Venetoclax-resistant AML patients. Thus, the Skd3 disaggregase assays established in this study could provide a powerful platform for isolating therapeutic compounds for MGCA7 and AML.

bioRxiv preprint doi: https://doi.org/10.1101/2020.01.17.911016; this version posted January 18, 2020. The copyright holder for this preprint (which was not certified by peer review) is the author/funder. All rights reserved. No reuse allowed without permission.

MATERIALS AND METHODS

Multiple Sequence Alignments

Sequences were acquired via SMART protein domain annotation resource (Letunic and Bork, 2018). Sequences from *Anolis carolinensis*, *Bos taurus*, *Callithrix jacchus*, *Canis lupus*, *Capra hircus*, *Danio rerio*, *Equus caballus*, *Geospiza fortis*, *Gorilla gorilla*, *Homo sapiens*, *Monosigia brevicollis*, *Mus musculus*, *Nothobranchius rachovii*, *Rattus norvegicus*, *Sus scrofa*, *Trachymyrmex septentrionalis*, *Trichinella papuae*, and *Xenopus laevis* were used to generate alignment for Fig. 1 and Extended Data Fig. 2. Compiled sequences were aligned and made into a guide tree via Clustal Omega (Madeira et al., 2019). Alignment image was generated via BoxShade tool (Hofmann, 1996). Guide tree image was built using FigTree (Rambaut, 2012). Species images were used under license via PhyloPic. Sequence logo was created using WebLogo and 42 mammalian Skd3 protein sequences (*Ailuropoda melanoleuca*, *Callorhinus ursinus*, *Canis lupus*, *Carlito syrichta*, *Cebus capucinus*, *Ceratotherium simum*, *Cercocebus atys*, *Chlorocebus sabaeus*, *Colobus angolensis*, *Equus asinus, Equus caballus*, *Equus przewalskii*, *Felis catus*, *Gorilla gorilla*, *Gulo gulo*, *Grammomys surdaster*, *Homo sapiens*, *Macaca fascicularis*, *Macaca mulatta*, *Macaca nemestrina*, *Mandrillus leucophaeus*, *Microcebus murinus*, *Microtus ochrogaster*, *Mustela putorius*, *Nomascus leucogenys*, *Odobenus rosmarus*, *Orycteropus afer*, *Pan paniscus*, *Pan troglodyte*, *Panthera tigris*, *Papio anubis*, *Piliocolobus tephrosceles*, *Pongo abelii*, *Propithecus coquereli*, *Puma concolor*, *Rhinopithecus bieti*, *Rhinopithecus roxellana*, *Rousettus aegyptiacus*, *Theropithecus gelada*, *Ursus arctos*, *Ursus maritimus*, and *Zalophus californianus*) (Crooks et al., 2004; Schneider and Stephens, 1990).

Cloning MBP-Skd3 Plasmids

bioRxiv preprint doi: https://doi.org/10.1101/2020.01.17.911016; this version posted January 18, 2020. The copyright holder for this preprint (which was not certified by peer review) is the author/funder. All rights reserved. No reuse allowed without permission.

$_{MPP}$Skd3, $_{PARL}$Skd3, $_{ANK}$Skd3, and $_{NBD2}$Skd3 were cloned into the pMAL C2 plasmid with TEV site (Yoshizawa et al., 2018) using Gibson assembly (Gibson et al., 2009). Site-directed mutagenesis was performed using QuikChange site-directed mutagenesis (Agilent) and confirmed by DNA sequencing.

Purification of Skd3

Skd3 variants were expressed as an N-terminally MBP-tagged protein in BL21 (DE3) RIL cells (Agilent). Cells were lysed via sonication in 40mM HEPES-KOH pH=7.4, 500mM KCl, 20% (w/v) glycerol, 5mM ATP, 10mM $MgCl_2$, 2mM β-mercaptoethanol, 2.5μM PepstatinA, and cOmplete Protease Inhibitor Cocktail (1 tablet/250mL, Millipore Sigma). Lysates were centrifuged at 30,597xg and 4°C for 20min and the supernatant was applied to amylose resin (NEB). The column was washed with 10 column volumes (CV) of wash buffer (WB: 40mM HEPES-KOH pH=7.4, 500mM KCl, 20% (w/v) glycerol, 5mM ATP, 10mM $MgCl_2$, 2mM β-mercaptoethanol, 2.5μM PepstatinA, and cOmplete Protease Inhibitor Cocktail) at 4°C, 3 CV of WB supplemented with 20mM ATP at 25°C for 30min, and 10 CV of WB at 4°C. The protein was then exchanged into elution buffer (EB: 50mM Tris-HCl pH=8.0, 300mM KCl, 10% glycerol, 5mM ATP, 10 mM $MgCl_2$, and 2mM β-mercaptoethanol) with 4 CV and eluted via TEV cleavage at 34°C. The protein was then run over a size exclusion column (GE Healthcare HiPrep™ 26/60 Sephacryl S-300 HR) in sizing buffer (50mM Tris-HCl pH=8.0, 500mM KCl, 10% glycerol, 1mM ATP, 10mM $MgCl_2$, and 1mM DTT). Peak fractions were collected, concentrated to >5mg/mL, supplemented with 5mM ATP, and snap frozen. Protein purity was determined to be > 95% by SDS-PAGE and Coomassie staining.

bioRxiv preprint doi: https://doi.org/10.1101/2020.01.17.911016; this version posted January 18, 2020. The copyright holder for this preprint (which was not certified by peer review) is the author/funder. All rights reserved. No reuse allowed without permission.

Purification of Hsp104

Hsp104 was purified as previously described (DeSantis et al., 2014). In brief, Hsp104 was expressed in BL21(DE3) RIL cells, lysed via sonication in lysis buffer [50mM Tris-HCl pH=8.0, 10mM $MgCl_2$, 2.5% glycerol, 2mM β-mercaptoethanol, 2.5μM PepstatinA, and cOmplete Protease Inhibitor Cocktail (1 mini EDTA-free tablet/50mL, Millipore Sigma)], clarified via centrifugation at 30,597xg and 4°C for 20min, and purified on Affi-Gel Blue Gel (Bio-Rad). Hsp104 was eluted in elution buffer (50mM Tris-HCl pH=8.0, 1M KCl, 10mM $MgCl_2$, 2.5% glycerol, and 2mM β-mercaptoethanol) and then exchanged into storage buffer (40mM HEPES-KOH pH=7.4, 500mM KCl, 20mM $MgCl_2$, 10% glycerol, 1mM DTT). The protein was diluted to 10% in buffer Q (20mM Tris-HCl pH=8.0, 50mM NaCl, 5mM $MgCl_2$, and 0.5mM EDTA) and loaded onto a 5mL RESOURCE Q anion exchange chromatography (GE Healthcare). Hsp104 was eluted via linear gradient of buffer Q+ (20mM Tris pH=8.0, 1M NaCl, 5mM $MgCl_2$, and 0.5mM EDTA). The protein was then exchanged into storage buffer and snap frozen. Protein purity was determined to be > 95% by SDS-PAGE and Coomassie staining.

Purification of Hsc70 and Hdj1

Hsc70 and Hdj1 were purified as previously described (Michalska et al., 2019). Hsc70 and Hdj1 were expressed in BL21 (DE3) RIL cells with an N-terminal His-SUMO tag. Cells were lysed via sonication into lysis buffer [50 mM HEPES-KOH pH=7.5, 750 mM KCl, 5 mM $MgCl_2$, 10% glycerol, 20 mM imidazole, 2 mM β-mercaptoethanol, 5 μM pepstatin A, and cOmplete Protease Inhibitor Cocktail (1 mini EDTA-free tablet/50mL)]. Lysates were centrifuged at 30,597xg and 4°C for 20min and the supernatant was bound to Ni-NTA Agarose resin (Qiagen), washed with 10 CV of wash buffer (50 mM HEPES-KOH pH=7.5, 750 mM KCl, 10 mM $MgCl_2$, 10%

bioRxiv preprint doi: https://doi.org/10.1101/2020.01.17.911016; this version posted January 18, 2020. The copyright holder for this preprint (which was not certified by peer review) is the author/funder. All rights reserved. No reuse allowed without permission.

glycerol, 20 mM imidazole, 1 mM ATP, and 2 mM β-mercaptoethanol), and then eluted with 2 CV of elution buffer (wash buffer supplemented with 300 mM imidazole). The tag was removed via Ulp1 (1:100 Ulp1:Protein molar ratio) cleavage during dialysis into wash buffer. The protein was further purified via loading onto a 5mL HisTrap HP column (GE Healthcare) and pooling the untagged elution. Cleaved protein was pooled, concentrated, purified further by Resource Q ion exchange chromatography, and snap frozen. Protein purity was determined to be > 95% by SDS-PAGE and Coomassie staining.

ATPase Assays

Proteins (0.25 μM monomer) were incubated with ATP (1mM) (Innova Biosciences) at 37°C for 5 min (or otherwise indicated) in luciferase reactivation buffer (LRB; 25 mM HEPES-KOH [pH=8.0], 150 mM KAOc, 10 mM MgAOc 10 mM DTT). For substrate-stimulation of ATPase activity the indicated concentration of substrate was added. ATPase activity was assessed via inorganic phosphate release with a malachite green detection assay (Expedeon) and measured in Nunc 96 Well Optical plates on a Tecan Infinite M1000 plate reader. Background hydrolysis was measured at time zero and subtracted (DeSantis et al., 2012).

Luciferase Disaggregation and Reactivation Assays

Firefly luciferase aggregates were formed by incubating luciferase (50μM) in LRB plus 8M urea at 30°C for 30 min. The luciferase was then rapidly diluted 100-fold into LRB, snap frozen, and stored at -80°C until use. Hsp104 and Skd3 variants (1 μM monomer, unless otherwise indicated) were incubated with 50 nM aggregated firefly luciferase in the presence or absence of Hsc70 and Hdj2 (0.167 μM each) in LRB plus 5 mM ATP plus an ATP regeneration system

bioRxiv preprint doi: https://doi.org/10.1101/2020.01.17.911016; this version posted January 18, 2020. The copyright holder for this preprint (which was not certified by peer review) is the author/funder. All rights reserved. No reuse allowed without permission.

(ARS; 1 mM creatine phosphate and 0.25 μM creatine kinase) at 37°C for 90 minutes (unless otherwise indicated). The nucleotide-dependence of Skd3 disaggregation activity was tested in the presence of ATP (Sigma), AMP-PNP (Roche), ATPγS (Roche), or ADP (MP Biomedicals) for 30 min at 37°C without ARS. Recovered luminescence was monitored in Nunc 96 Well Optical plates using a Tecan Infinite M1000 plate reader (DeSantis et al., 2012).

α-Synuclein Disaggregation Assay

α-Synuclein fibrils were acquired from the Luk lab and formed as previously described (Luk et al., 2012). PARLSkd3 (10μM monomer) was incubated with α-synuclein fibrils (0.5μM monomer) in LRB in the presence or absence of ARS (10mM ATP, 10mM creatine phosphate, 40μg/mL creatine kinase) at 37°C for 90 minutes. The samples were then centrifuged at 4°C and 20,000xg for 20 minutes. After centrifugation the supernatants were pipetted off of the pellets and the pellets were boiled in Pellet Buffer (PB; 50mM Tris-HCl [pH=8.0], 8M Urea, 150mM NaCl, 10uL/1mL mammalian PI cocktail [Sigma CAT# P8340]) for 5 minutes at 99°C. The total sample, supernatant, and pellet samples were then blotted on nitrocellulose membrane (ThermoFisher Scientific CAT# 88018) and incubated with the SYN211 antibody (ThermoFisher Scientific CAT# AHB0261). Blots were then incubated with the IRDye® 800CW Goat anti-Mouse IgG Secondary Antibody (Li-COR CAT# 926-32210) and imaged using the Li-Cor Odyssey® Fc Imaging System. Samples were quantified using FIJI and normalized as (signal in supernatant)/(signal in pellet + signal in supernatant).

Western Blots

bioRxiv preprint doi: https://doi.org/10.1101/2020.01.17.911016; this version posted January 18, 2020. The copyright holder for this preprint (which was not certified by peer review) is the author/funder. All rights reserved. No reuse allowed without permission.

Mammalian whole cell lysates were prepared by boiling 500,000 cells in 1x Sample Buffer (SB; 60mM Tris-HCl [pH=6.8], 5% glycerol, 2% SDS, 10% β-mercaptoethanol, 0.025% bromophenol blue, 1x Mammalian PI cocktail) for 5 min at 99°C. Sedimentation assay samples were prepared as described above. Western blot samples were boiled for 5 min at 99°C in 1x SB, separated by SDS-PAGE on a gradient gel (4%–20%, Bio-Rad CAT# 3450033), and transferred to a PVDF membrane. Membranes were blocked in Odyssey® Blocking Buffer in PBS (Li-Cor CAT# 927-40000) for 1 hour at 25°C. Blots were then incubated in primary antibody overnight at 4°C and then in secondary for 30 min at 25°C. The antibodies used were: α-CLPB (Abcam CAT# ab235349), α-HAX1 (Abcam CAT# ab137613), α-COXIV (Abcam CAT# ab14744), IRDye® 800CW Goat α-mouse secondary (Li-Cor CAT# 926-32210), and IRDye 680RD Goat α-rabbit secondary (Li-Cor CAT# 926-68071). Blots were imaged on a Li-Cor Odyssey® Fc Imaging System.

Mammalian Cell Culture

Isogenic HAP1 and HAP1 Δ*CLPB* cells were acquired from Horizon Discovery and knockout was confirmed via Western blot. Cells were maintained in IMDM (Gibco CAT# 12440053) supplemented with 10% FBS (GE CAT# SH3007003) and 1% P/S (Gibco CAT# 15140122) at 37°C and 5% CO_2. Cells were grown at a confluency of 50-60% for mitochondrial isolation.

Mitochondrial Isolation

Mitochondria were isolated as previously described (Frezza et al., 2007). In brief, 50-100*10^6 cells were resuspended in 5mL SM buffer (50mM Tris-HCl [pH=7.4], 0.25M sucrose, 2mM EDTA, and 1% BSA) and homogenized with a Dounce homogenizer and Teflon pestle (30

bioRxiv preprint doi: https://doi.org/10.1101/2020.01.17.911016; this version posted January 18, 2020. The copyright holder for this preprint (which was not certified by peer review) is the author/funder. All rights reserved. No reuse allowed without permission.

strokes at 600 RPM) at 4°C. Lysate was then centrifuged at 600xg for 10 minutes. The supernatant was collected, and the pellet was dissolved in 5mL SM buffer and homogenized (15 strokes at 600 RPM). Sample was then centrifuged at 600xg for 10 minutes and the supernatant was pooled and centrifuged at 12,000xg for 15 min. The pellet was collected and used for further experiments.

Mitochondrial Sedimentation Assay

Mitochondrial sedimentation assay was performed essentially as previously described (Wilkening et al., 2018). 60-80µg isolated mitochondria were resuspended in 200µL Mitochondrial Resuspension Buffer (40mM HEPES-KOH, pH=7.6, 500mM sucrose, 120mM K-acetate, 10mM Mg-acetate, 5mM glutamate, 5mM malate, 5mM EDTA, 5mM ATP, 20mM creatine phosphate, 4 µg/mL creatine kinase, 1mM DTT) and incubated at 37°C for 20min. The mitochondria were then pelleted at 12,000xg for 10 min at 4°C. The mitochondria were then resuspended in 200µL Lysis Buffer (30mM Tris-HCl, pH=7.4, 200mM KCl, 0.5% v/v Triton X-100, 5mM EDTA, 0.5mM PMSF, 1x Mammalian PI cocktail) and lysed in a thermomixer at 2,000 RPM for 10 min at 4°C. The protein concentration of the lysate was then quantified using a BCA assay (ThermoFisher CAT# 23225). 12µg of lysate was added to a total volume of 50µL Lysis Buffer and reserved as a total protein sample. 12µg of lysate was added to a total volume of 50µL Lysis Buffer and sedimented at 20,000xg for 20min at 4°C. The supernatant was removed, TCA precipitated, and frozen for later processing. The pellet was boiled in 10µL of Pellet Buffer and frozen for later processing.

Mass Spectrometry

bioRxiv preprint doi: https://doi.org/10.1101/2020.01.17.911016; this version posted January 18, 2020. The copyright holder for this preprint (which was not certified by peer review) is the author/funder. All rights reserved. No reuse allowed without permission.

Pellet samples were excised as whole lanes from gels, reduced with TCEP, alkylated with iodoacetamide, and digested with trypsin. Tryptic digests were desalted by loading onto a MonoCap C18 Trap Column (GL Sciences), flushed for 5 min at 6µL/min using 100% Buffer A (H_20, 0.1% formic acid), then analyzed via LC (Waters NanoAcquity) gradient using Buffer A and Buffer B (acetonitrile, 0.1% formic acid) (initial 5% B; 75 min 30% B; 80 min 80% B; 90.5-105 min 5% B) on the Thermo Q Exactive HF mass spectrometer. Data were acquired in data-dependent mode. Analysis was performed with the following settings: MS1 60K resolution, AGC target 3e6, max inject time 50 ms; MS2 Top N = 20 15K resolution, AGC target 5e4, max inject time 50 ms, isolation window = 1.5 m/z, normalized collision energy 28%. LC-MS/MS data were searched with full tryptic specificity against the UniProt human database using MaxQuant 1.6.8.0. MS data were also searched for common protein N-terminal acetylation and methionine oxidation. Protein and peptide false discovery rate was set at 1%. LFQ intensity was calculated using the MaxLFQ algorithm (Cox et al., 2014). Fold enrichment was calculated as LFQ intensity from the Δ*CLPB* pellet divided by the LFQ intensity from the wild-type pellet. High confidence hits were quantified as minimum absolute fold change of 2 and p-value <0.05.

bioRxiv preprint doi: https://doi.org/10.1101/2020.01.17.911016; this version posted January 18, 2020. The copyright holder for this preprint (which was not certified by peer review) is the author/funder. All rights reserved. No reuse allowed without permission.

ACKNOWLEDGEMENTS

We thank Kelvin Luk, Douglas C. Wallace, Prasanth Potluri, and Manisha Koneru for generously providing key reagents. We thank the Wistar Institute Proteomics & Metabolomics Facility for their assistance with the LC-MS/MS experiments, especially Hsin-Yao Tang and Thomas Beer. We thank Edward Barbieri, Edward Chuang, Jordan Cupo, Albert Erives, Jan Fassler, Charlotte Fare, Oliver King, JiaBei Lin, Dylan Marchione, Zachary March, Hana Odeh, April Darling, and Bede Portz for feedback on the manuscript. Our work was funded by the Blavatnik Family Foundation Fellowship (R.R.C.) and NIH grants T32GM008275 (R.R.C.), F31AG060672 (R.R.C.), and R01GM099836 (J.S.).

bioRxiv preprint doi: https://doi.org/10.1101/2020.01.17.911016; this version posted January 18, 2020. The copyright holder for this preprint (which was not certified by peer review) is the author/funder. All rights reserved. No reuse allowed without permission.

REFERENCES

Angebault, C., Charif, M., Guegen, N., Piro-Megy, C., Mousson de Camaret, B., Procaccio, V., Guichet, P.O., Hebrard, M., Manes, G., Leboucq, N., Rivier, F., Hamel, C.P., Lenaers, G., and Roubertie, A. (2015). Mutation in NDUFA13/GRIM19 leads to early onset hypotonia, dyskinesia and sensorial deficiencies, and mitochondrial complex I instability. Hum Mol Genet *24*, 3948-3955.

Ashburner, M., Ball, C.A., Blake, J.A., Botstein, D., Butler, H., Cherry, J.M., Davis, A.P., Dolinski, K., Dwight, S.S., Eppig, J.T., Harris, M.A., Hill, D.P., Issel-Tarver, L., Kasarskis, A., Lewis, S., Matese, J.C., Richardson, J.E., Ringwald, M., Rubin, G.M., and Sherlock, G. (2000). Gene ontology: tool for the unification of biology. The Gene Ontology Consortium. Nat Genet *25*, 25-29.

Bateman, J.M., Iacovino, M., Perlman, P.S., and Butow, R.A. (2002). Mitochondrial DNA instability mutants of the bifunctional protein Ilv5p have altered organization in mitochondria and are targeted for degradation by Hsp78 and the Pim1p protease. J Biol Chem *277*, 47946-47953.

Baumann, U., Fernandez-Saiz, V., Rudelius, M., Lemeer, S., Rad, R., Knorn, A.M., Slawska, J., Engel, K., Jeremias, I., Li, Z., Tomiatti, V., Illert, A.L., Targosz, B.S., Braun, M., Perner, S., Leitges, M., Klapper, W., Dreyling, M., Miething, C., Lenz, G., Rosenwald, A., Peschel, C., Keller, U., Kuster, B., and Bassermann, F. (2014). Disruption of the PRKCD-FBXO25-HAX-1 axis attenuates the apoptotic response and drives lymphomagenesis. Nat Med *20*, 1401-1409.

Beinker, P., Schlee, S., Auvula, R., and Reinstein, J. (2005). Biochemical coupling of the two nucleotide binding domains of ClpB: covalent linkage is not a prerequisite for chaperone activity. J Biol Chem *280*, 37965-37973.

Brunet, T., and King, N. (2017). The Origin of Animal Multicellularity and Cell Differentiation. Dev Cell *43*, 124-140.

Capo-Chichi, J.M., Boissel, S., Brustein, E., Pickles, S., Fallet-Bianco, C., Nassif, C., Patry, L., Dobrzeniecka, S., Liao, M., Labuda, D., Samuels, M.E., Hamdan, F.F., Vande Velde, C., Rouleau, G.A., Drapeau, P., and Michaud, J.L. (2015). Disruption of CLPB is associated with congenital microcephaly, severe encephalopathy and 3-methylglutaconic aciduria. J Med Genet *52*, 303-311.

Cashikar, A.G., Schirmer, E.C., Hattendorf, D.A., Glover, J.R., Ramakrishnan, M.S., Ware, D.M., and Lindquist, S.L. (2002). Defining a pathway of communication from the C-terminal peptide binding domain to the N-terminal ATPase domain in a AAA protein. Mol Cell *9*, 751-760.

Chacinska, A., Lind, M., Frazier, A.E., Dudek, J., Meisinger, C., Geissler, A., Sickmann, A., Meyer, H.E., Truscott, K.N., Guiard, B., Pfanner, N., and Rehling, P. (2005). Mitochondrial presequence translocase: switching between TOM tethering and motor recruitment involves Tim21 and Tim17. Cell *120*, 817-829.

bioRxiv preprint doi: https://doi.org/10.1101/2020.01.17.911016; this version posted January 18, 2020. The copyright holder for this preprint (which was not certified by peer review) is the author/funder. All rights reserved. No reuse allowed without permission.

Chai, J., Du, C., Wu, J.W., Kyin, S., Wang, X., and Shi, Y. (2000). Structural and biochemical basis of apoptotic activation by Smac/DIABLO. Nature *406*, 855-862.

Chao, J.R., Parganas, E., Boyd, K., Hong, C.Y., Opferman, J.T., and Ihle, J.N. (2008). Hax1-mediated processing of HtrA2 by Parl allows survival of lymphocytes and neurons. Nature *452*, 98-102.

Chen, X., Glytsou, C., Zhou, H., Narang, S., Reyna, D.E., Lopez, A., Sakellaropoulos, T., Gong, Y., Kloetgen, A., Yap, Y.S., Wang, E., Gavathiotis, E., Tsirigos, A., Tibes, R., and Aifantis, I. (2019). Targeting Mitochondrial Structure Sensitizes Acute Myeloid Leukemia to Venetoclax Treatment. Cancer Discov *9*, 890-909.

Chuang, E., Hori, A.M., Hesketh, C.D., and Shorter, J. (2018). Amyloid assembly and disassembly. J Cell Sci *131*.

Cipolat, S., Rudka, T., Hartmann, D., Costa, V., Serneels, L., Craessaerts, K., Metzger, K., Frezza, C., Annaert, W., D'Adamio, L., Derks, C., Dejaegere, T., Pellegrini, L., D'Hooge, R., Scorrano, L., and De Strooper, B. (2006). Mitochondrial rhomboid PARL regulates cytochrome c release during apoptosis via OPA1-dependent cristae remodeling. Cell *126*, 163-175.

Claros, M.G., and Vincens, P. (1996). Computational method to predict mitochondrially imported proteins and their targeting sequences. Eur J Biochem *241*, 779-786.

Couvillion, M.T., Soto, I.C., Shipkovenska, G., and Churchman, L.S. (2016). Synchronized mitochondrial and cytosolic translation programs. Nature *533*, 499-503.

Cox, J., Hein, M.Y., Luber, C.A., Paron, I., Nagaraj, N., and Mann, M. (2014). Accurate proteome-wide label-free quantification by delayed normalization and maximal peptide ratio extraction, termed MaxLFQ. Mol Cell Proteomics *13*, 2513-2526.

Crooks, G.E., Hon, G., Chandonia, J.M., and Brenner, S.E. (2004). WebLogo: a sequence logo generator. Genome Res *14*, 1188-1190.

Csordas, G., Golenar, T., Seifert, E.L., Kamer, K.J., Sancak, Y., Perocchi, F., Moffat, C., Weaver, D., de la Fuente Perez, S., Bogorad, R., Koteliansky, V., Adijanto, J., Mootha, V.K., and Hajnoczky, G. (2013). MICU1 controls both the threshold and cooperative activation of the mitochondrial Ca(2)(+) uniporter. Cell Metab *17*, 976-987.

Cushman-Nick, M., Bonini, N.M., and Shorter, J. (2013). Hsp104 suppresses polyglutamine-induced degeneration post onset in a Drosophila MJD/SCA3 model. PLoS Genet *9*, e1003781.

Dandoy-Dron, F., Bogdanova, A., Beringue, V., Bailly, Y., Tovey, M.G., Laude, H., and Dron, M. (2006). Infection by ME7 prion is not modified in transgenic mice expressing the yeast chaperone Hsp104 in neurons. Neurosci Lett *405*, 181-185.

DeSantis, M.E., Leung, E.H., Sweeny, E.A., Jackrel, M.E., Cushman-Nick, M., Neuhaus-Follini, A., Vashist, S., Sochor, M.A., Knight, M.N., and Shorter, J. (2012). Operational plasticity enables hsp104 to disaggregate diverse amyloid and nonamyloid clients. Cell *151*, 778-793.

bioRxiv preprint doi: https://doi.org/10.1101/2020.01.17.911016; this version posted January 18, 2020. The copyright holder for this preprint (which was not certified by peer review) is the author/funder. All rights reserved. No reuse allowed without permission.

DeSantis, M.E., Sweeny, E.A., Snead, D., Leung, E.H., Go, M.S., Gupta, K., Wendler, P., and Shorter, J. (2014). Conserved distal loop residues in the Hsp104 and ClpB middle domain contact nucleotide-binding domain 2 and enable Hsp70-dependent protein disaggregation. J Biol Chem *289*, 848-867.

Donzeau, M., Kaldi, K., Adam, A., Paschen, S., Wanner, G., Guiard, B., Bauer, M.F., Neupert, W., and Brunner, M. (2000). Tim23 links the inner and outer mitochondrial membranes. Cell *101*, 401-412.

Eisele, Y.S., Monteiro, C., Fearns, C., Encalada, S.E., Wiseman, R.L., Powers, E.T., and Kelly, J.W. (2015). Targeting protein aggregation for the treatment of degenerative diseases. Nat Rev Drug Discov *14*, 759-780.

Erives, A., and Fassler, J. (2015). Metabolic and chaperone gene loss marks the origin of animals: evidence for hsp104 and hsp78 chaperones sharing mitochondrial enzymes as clients. PLoS One *10*.

Erzberger, J.P., and Berger, J.M. (2006). Evolutionary relationships and structural mechanisms of AAA+ proteins. Annu Rev Biophys Biomol Struct *35*, 93-114.

Frezza, C., Cipolat, S., Martins de Brito, O., Micaroni, M., Beznoussenko, G.V., Rudka, T., Bartoli, D., Polishuck, R.S., Danial, N.N., De Strooper, B., and Scorrano, L. (2006). OPA1 controls apoptotic cristae remodeling independently from mitochondrial fusion. Cell *126*, 177-189.

Frezza, C., Cipolat, S., and Scorrano, L. (2007). Organelle isolation: functional mitochondria from mouse liver, muscle and cultured fibroblasts. Nat Protoc *2*, 287-295.

Gates, S.N., Yokom, A.L., Lin, J., Jackrel, M.E., Rizo, A.N., Kendsersky, N.M., Buell, C.E., Sweeny, E.A., Mack, K.L., Chuang, E., Torrente, M.P., Su, M., Shorter, J., and Southworth, D.R. (2017). Ratchet-like polypeptide translocation mechanism of the AAA+ disaggregase Hsp104. Science *357*, 273-279.

Geissler, A., Chacinska, A., Truscott, K.N., Wiedemann, N., Brandner, K., Sickmann, A., Meyer, H.E., Meisinger, C., Pfanner, N., and Rehling, P. (2002). The mitochondrial presequence translocase: an essential role of Tim50 in directing preproteins to the import channel. Cell *111*, 507-518.

Germaniuk, A., Liberek, K., and Marszalek, J. (2002). A bichaperone (Hsp70-Hsp78) system restores mitochondrial DNA synthesis following thermal inactivation of Mip1p polymerase. J Biol Chem *277*, 27801-27808.

Ghezzi, D., Arzuffi, P., Zordan, M., Da Re, C., Lamperti, C., Benna, C., D'Adamo, P., Diodato, D., Costa, R., Mariotti, C., Uziel, G., Smiderle, C., and Zeviani, M. (2011). Mutations in TTC19 cause mitochondrial complex III deficiency and neurological impairment in humans and flies. Nat Genet *43*, 259-263.

bioRxiv preprint doi: https://doi.org/10.1101/2020.01.17.911016; this version posted January 18, 2020. The copyright holder for this preprint (which was not certified by peer review) is the author/funder. All rights reserved. No reuse allowed without permission.

Gibson, D.G., Young, L., Chuang, R.Y., Venter, J.C., Hutchison, C.A., 3rd, and Smith, H.O. (2009). Enzymatic assembly of DNA molecules up to several hundred kilobases. Nat Methods *6*, 343-345.

Glover, J.R., and Lindquist, S. (1998). Hsp104, Hsp70, and Hsp40: a novel chaperone system that rescues previously aggregated proteins. Cell *94*, 73-82.

Goloubinoff, P., Mogk, A., Zvi, A.P., Tomoyasu, T., and Bukau, B. (1999). Sequential mechanism of solubilization and refolding of stable protein aggregates by a bichaperone network. Proc Natl Acad Sci U S A *96*, 13732-13737.

Greber, B.J., and Ban, N. (2016). Structure and Function of the Mitochondrial Ribosome. Annu Rev Biochem *85*, 103-132.

Guo, L., Fare, C.M., and Shorter, J. (2019). Therapeutic Dissolution of Aberrant Phases by Nuclear-Import Receptors. Trends Cell Biol *29*, 308-322.

Guo, L., Kim, H.J., Wang, H., Monaghan, J., Freyermuth, F., Sung, J.C., O'Donovan, K., Fare, C.M., Diaz, Z., Singh, N., Zhang, Z.C., Coughlin, M., Sweeny, E.A., DeSantis, M.E., Jackrel, M.E., Rodell, C.B., Burdick, J.A., King, O.D., Gitler, A.D., Lagier-Tourenne, C., Pandey, U.B., Chook, Y.M., Taylor, J.P., and Shorter, J. (2018). Nuclear-Import Receptors Reverse Aberrant Phase Transitions of RNA-Binding Proteins with Prion-like Domains. Cell *173*, 677-692 e620.

Hanson, P.I., and Whiteheart, S.W. (2005). AAA+ proteins: have engine, will work. Nat Rev Mol Cell Biol *6*, 519-529.

Hattendorf, D.A., and Lindquist, S.L. (2002). Analysis of the AAA sensor-2 motif in the C-terminal ATPase domain of Hsp104 with a site-specific fluorescent probe of nucleotide binding. Proc Natl Acad Sci U S A *99*, 2732-2737.

Henderson, M.X., Trojanowski, J.Q., and Lee, V.M. (2019). alpha-Synuclein pathology in Parkinson's disease and related alpha-synucleinopathies. Neurosci Lett *709*, 134316.

Hofmann, K., and M. D. Baron (1996). Boxshade 3.21. In Pretty printing and shading of multiple-alignment files (Kay Hofmann, ISREC Bioinformatics Group, Lausanne, Switzerland).

Jackrel, M.E., DeSantis, M.E., Martinez, B.A., Castellano, L.M., Stewart, R.M., Caldwell, K.A., Caldwell, G.A., and Shorter, J. (2014). Potentiated Hsp104 variants antagonize diverse proteotoxic misfolding events. Cell *156*, 170-182.

Jackrel, M.E., and Shorter, J. (2014). Potentiated Hsp104 variants suppress toxicity of diverse neurodegenerative disease-linked proteins. Dis Model Mech *7*, 1175-1184.

Jackrel, M.E., Yee, K., Tariq, A., Chen, A.I., and Shorter, J. (2015). Disparate Mutations Confer Therapeutic Gain of Hsp104 Function. ACS Chem Biol *10*, 2672-2679.

Jaru-Ampornpan, P., Liang, F.C., Nisthal, A., Nguyen, T.X., Wang, P., Shen, K., Mayo, S.L., and Shan, S.O. (2013). Mechanism of an ATP-independent protein disaggregase: II. distinct

bioRxiv preprint doi: https://doi.org/10.1101/2020.01.17.911016; this version posted January 18, 2020. The copyright holder for this preprint (which was not certified by peer review) is the author/funder. All rights reserved. No reuse allowed without permission.

molecular interactions drive multiple steps during aggregate disassembly. J Biol Chem *288*, 13431-13445.

Jaru-Ampornpan, P., Shen, K., Lam, V.Q., Ali, M., Doniach, S., Jia, T.Z., and Shan, S.O. (2010). ATP-independent reversal of a membrane protein aggregate by a chloroplast SRP subunit. Nat Struct Mol Biol *17*, 696-702.

Kanabus, M., Shahni, R., Saldanha, J.W., Murphy, E., Plagnol, V., Hoff, W.V., Heales, S., and Rahman, S. (2015). Bi-allelic CLPB mutations cause cataract, renal cysts, nephrocalcinosis and 3-methylglutaconic aciduria, a novel disorder of mitochondrial protein disaggregation. J Inherit Metab Dis *38*, 211-219.

Kiykim, A., Garncarz, W., Karakoc-Aydiner, E., Ozen, A., Kiykim, E., Yesil, G., Boztug, K., and Baris, S. (2016). Novel CLPB mutation in a patient with 3-methylglutaconic aciduria causing severe neurological involvement and congenital neutropenia. Clin Immunol *165*, 1-3.

Klein, C., Grudzien, M., Appaswamy, G., Germeshausen, M., Sandrock, I., Schaffer, A.A., Rathinam, C., Boztug, K., Schwinzer, B., Rezaei, N., Bohn, G., Melin, M., Carlsson, G., Fadeel, B., Dahl, N., Palmblad, J., Henter, J.I., Zeidler, C., Grimbacher, B., and Welte, K. (2007). HAX1 deficiency causes autosomal recessive severe congenital neutropenia (Kostmann disease). Nat Genet *39*, 86-92.

Krzewska, J., Langer, T., and Liberek, K. (2001). Mitochondrial Hsp78, a member of the Clp/Hsp100 family in Saccharomyces cerevisiae, cooperates with Hsp70 in protein refolding. FEBS Lett *489*, 92-96.

Kyte, J., and Doolittle, R.F. (1982). A simple method for displaying the hydropathic character of a protein. J Mol Biol *157*, 105-132.

Lee, J., Kim, J.H., Biter, A.B., Sielaff, B., Lee, S., and Tsai, F.T. (2013). Heat shock protein (Hsp) 70 is an activator of the Hsp104 motor. Proc Natl Acad Sci U S A *110*, 8513-8518.

Letunic, I., and Bork, P. (2018). 20 years of the SMART protein domain annotation resource. Nucleic Acids Res *46*, D493-D496.

Lo Bianco, C., Shorter, J., Regulier, E., Lashuel, H., Iwatsubo, T., Lindquist, S., and Aebischer, P. (2008). Hsp104 antagonizes alpha-synuclein aggregation and reduces dopaminergic degeneration in a rat model of Parkinson disease. J Clin Invest *118*, 3087-3097.

Luk, K.C., Kehm, V., Carroll, J., Zhang, B., O'Brien, P., Trojanowski, J.Q., and Lee, V.M. (2012). Pathological alpha-synuclein transmission initiates Parkinson-like neurodegeneration in nontransgenic mice. Science *338*, 949-953.

Lum, R., Niggemann, M., and Glover, J.R. (2008). Peptide and protein binding in the axial channel of Hsp104. Insights into the mechanism of protein unfolding. J Biol Chem *283*, 30139-30150.

bioRxiv preprint doi: https://doi.org/10.1101/2020.01.17.911016; this version posted January 18, 2020. The copyright holder for this preprint (which was not certified by peer review) is the author/funder. All rights reserved. No reuse allowed without permission.

Lum, R., Tkach, J.M., Vierling, E., and Glover, J.R. (2004). Evidence for an unfolding/threading mechanism for protein disaggregation by Saccharomyces cerevisiae Hsp104. J Biol Chem *279*, 29139-29146.

Madeira, F., Park, Y.M., Lee, J., Buso, N., Gur, T., Madhusoodanan, N., Basutkar, P., Tivey, A.R.N., Potter, S.C., Finn, R.D., and Lopez, R. (2019). The EMBL-EBI search and sequence analysis tools APIs in 2019. Nucleic Acids Res *47*, W636-W641.

Mattoo, R.U., Sharma, S.K., Priya, S., Finka, A., and Goloubinoff, P. (2013). Hsp110 is a bona fide chaperone using ATP to unfold stable misfolded polypeptides and reciprocally collaborate with Hsp70 to solubilize protein aggregates. J Biol Chem *288*, 21399-21411.

McAvoy, C.Z., Siegel, A., Piszkiewicz, S., Miaou, E., Yu, M., Nguyen, T., Moradian, A., Sweredoski, M.J., Hess, S., and Shan, S.O. (2018). Two distinct sites of client protein interaction with the chaperone cpSRP43. J Biol Chem *293*, 8861-8873.

Meinecke, M., Wagner, R., Kovermann, P., Guiard, B., Mick, D.U., Hutu, D.P., Voos, W., Truscott, K.N., Chacinska, A., Pfanner, N., and Rehling, P. (2006). Tim50 maintains the permeability barrier of the mitochondrial inner membrane. Science *312*, 1523-1526.

Mi, H., Muruganujan, A., Ebert, D., Huang, X., and Thomas, P.D. (2019). PANTHER version 14: more genomes, a new PANTHER GO-slim and improvements in enrichment analysis tools. Nucleic Acids Res *47*, D419-D426.

Michalska, K., Zhang, K., March, Z.M., Hatzos-Skintges, C., Pintilie, G., Bigelow, L., Castellano, L.M., Miles, L.J., Jackrel, M.E., Chuang, E., Jedrzejczak, R., Shorter, J., Chiu, W., and Joachimiak, A. (2019). Structure of Calcarisporiella thermophila Hsp104 Disaggregase that Antagonizes Diverse Proteotoxic Misfolding Events. Structure *27*, 449-463 e447.

Moczko, M., Schonfisch, B., Voos, W., Pfanner, N., and Rassow, J. (1995). The mitochondrial ClpB homolog Hsp78 cooperates with matrix Hsp70 in maintenance of mitochondrial function. J Mol Biol *254*, 538-543.

Mogk, A., Schlieker, C., Strub, C., Rist, W., Weibezahn, J., and Bukau, B. (2003). Roles of individual domains and conserved motifs of the AAA+ chaperone ClpB in oligomerization, ATP hydrolysis, and chaperone activity. J Biol Chem *278*, 17615-17624.

Mokranjac, D., Paschen, S.A., Kozany, C., Prokisch, H., Hoppins, S.C., Nargang, F.E., Neupert, W., and Hell, K. (2003). Tim50, a novel component of the TIM23 preprotein translocase of mitochondria. EMBO J *22*, 816-825.

Nguyen, T.X., Jaru-Ampornpan, P., Lam, V.Q., Cao, P., Piszkiewicz, S., Hess, S., and Shan, S.O. (2013). Mechanism of an ATP-independent protein disaggregase: I. structure of a membrane protein aggregate reveals a mechanism of recognition by its chaperone. J Biol Chem *288*, 13420-13430.

Niaki, A.G., Sarkar, J., Cai, X., Rhine, K., Vidaurre, V., Guy, B., Hurst, M., Lee, J.C., Koh, H.R., Guo, L., Fare, C.M., Shorter, J., and Myong, S. (2020). Loss of Dynamic RNA Interaction

bioRxiv preprint doi: https://doi.org/10.1101/2020.01.17.911016; this version posted January 18, 2020. The copyright holder for this preprint (which was not certified by peer review) is the author/funder. All rights reserved. No reuse allowed without permission.

and Aberrant Phase Separation Induced by Two Distinct Types of ALS/FTD-Linked FUS Mutations. Mol Cell *77*, 82-94 e84.

Nillegoda, N.B., Kirstein, J., Szlachcic, A., Berynskyy, M., Stank, A., Stengel, F., Arnsburg, K., Gao, X., Scior, A., Aebersold, R., Guilbride, D.L., Wade, R.C., Morimoto, R.I., Mayer, M.P., and Bukau, B. (2015). Crucial HSP70 co-chaperone complex unlocks metazoan protein disaggregation. Nature *524*, 247-251.

Parsell, D.A., Kowal, A.S., Singer, M.A., and Lindquist, S. (1994). Protein disaggregation mediated by heat-shock protein Hsp104. Nature *372*, 475-478.

Paschen, S.A., Rothbauer, U., Kaldi, K., Bauer, M.F., Neupert, W., and Brunner, M. (2000). The role of the TIM8-13 complex in the import of Tim23 into mitochondria. EMBO J *19*, 6392-6400.

Patron, M., Checchetto, V., Raffaello, A., Teardo, E., Vecellio Reane, D., Mantoan, M., Granatiero, V., Szabo, I., De Stefani, D., and Rizzuto, R. (2014). MICU1 and MICU2 finely tune the mitochondrial Ca2+ uniporter by exerting opposite effects on MCU activity. Mol Cell *53*, 726-737.

Perier, F., Radeke, C.M., Raab-Graham, K.F., and Vandenberg, C.A. (1995). Expression of a putative ATPase suppresses the growth defect of a yeast potassium transport mutant: identification of a mammalian member of the Clp/HSP104 family. Gene *152*, 157-163.

Perocchi, F., Gohil, V.M., Girgis, H.S., Bao, X.R., McCombs, J.E., Palmer, A.E., and Mootha, V.K. (2010). MICU1 encodes a mitochondrial EF hand protein required for Ca(2+) uptake. Nature *467*, 291-296.

Perrin, V., Regulier, E., Abbas-Terki, T., Hassig, R., Brouillet, E., Aebischer, P., Luthi-Carter, R., and Deglon, N. (2007). Neuroprotection by Hsp104 and Hsp27 in lentiviral-based rat models of Huntington's disease. Mol Ther *15*, 903-911.

Plovanich, M., Bogorad, R.L., Sancak, Y., Kamer, K.J., Strittmatter, L., Li, A.A., Girgis, H.S., Kuchimanchi, S., De Groot, J., Speciner, L., Taneja, N., Oshea, J., Koteliansky, V., and Mootha, V.K. (2013). MICU2, a paralog of MICU1, resides within the mitochondrial uniporter complex to regulate calcium handling. PLoS One *8*, e55785.

Pronicka, E., Ropacka-Lesiak, M., Trubicka, J., Pajdowska, M., Linke, M., Ostergaard, E., Saunders, C., Horsch, S., van Karnebeek, C., Yaplito-Lee, J., Distelmaier, F., Ounap, K., Rahman, S., Castelle, M., Kelleher, J., Baris, S., Iwanicka-Pronicka, K., Steward, C.G., Ciara, E., Wortmann, S.B., and Additional individual, c. (2017). A scoring system predicting the clinical course of CLPB defect based on the foetal and neonatal presentation of 31 patients. J Inherit Metab Dis *40*, 853-860.

Queitsch, C., Hong, S.W., Vierling, E., and Lindquist, S. (2000). Heat shock protein 101 plays a crucial role in thermotolerance in Arabidopsis. Plant Cell *12*, 479-492.

Rambaut, A. (2012). FigTree v1. 4.

bioRxiv preprint doi: https://doi.org/10.1101/2020.01.17.911016; this version posted January 18, 2020. The copyright holder for this preprint (which was not certified by peer review) is the author/funder. All rights reserved. No reuse allowed without permission.

Rottgers, K., Zufall, N., Guiard, B., and Voos, W. (2002). The ClpB homolog Hsp78 is required for the efficient degradation of proteins in the mitochondrial matrix. Journal of Biological Chemistry *277*, 45829-45837.

Saita, S., Nolte, H., Fiedler, K.U., Kashkar, H., Venne, A.S., Zahedi, R.P., Kruger, M., and Langer, T. (2017). PARL mediates Smac proteolytic maturation in mitochondria to promote apoptosis. Nat Cell Biol *19*, 318-328.

Satyal, S.H., Schmidt, E., Kitagawa, K., Sondheimer, N., Lindquist, S., Kramer, J.M., and Morimoto, R.I. (2000). Polyglutamine aggregates alter protein folding homeostasis in *Caenorhabditis elegans*. Proc Natl Acad Sci USA *97*, 5750-5755.

Saunders, C., Smith, L., Wibrand, F., Ravn, K., Bross, P., Thiffault, I., Christensen, M., Atherton, A., Farrow, E., Miller, N., Kingsmore, S.F., and Ostergaard, E. (2015). CLPB variants associated with autosomal-recessive mitochondrial disorder with cataract, neutropenia, epilepsy, and methylglutaconic aciduria. Am J Hum Genet *96*, 258-265.

Saurer, M., Ramrath, D.J.F., Niemann, M., Calderaro, S., Prange, C., Mattei, S., Scaiola, A., Leitner, A., Bieri, P., Horn, E.K., Leibundgut, M., Boehringer, D., Schneider, A., and Ban, N. (2019). Mitoribosomal small subunit biogenesis in trypanosomes involves an extensive assembly machinery. Science *365*, 1144-1149.

Schmitt, M., Neupert, W., and Langer, T. (1995). Hsp78, a Clp homologue within mitochondria, can substitute for chaperone functions of mt-hsp70. EMBO J *14*, 3434-3444.

Schmitt, M., Neupert, W., and Langer, T. (1996). The molecular chaperone Hsp78 confers compartment-specific thermotolerance to mitochondria. J Cell Biol *134*, 1375-1386.

Schneider, T.D., and Stephens, R.M. (1990). Sequence logos: a new way to display consensus sequences. Nucleic Acids Res *18*, 6097-6100.

Shorter, J. (2008). Hsp104: a weapon to combat diverse neurodegenerative disorders. Neurosignals *16*, 63-74.

Shorter, J. (2011). The mammalian disaggregase machinery: Hsp110 synergizes with Hsp70 and Hsp40 to catalyze protein disaggregation and reactivation in a cell-free system. PLoS One *6*, e26319.

Shorter, J. (2017). Designer protein disaggregases to counter neurodegenerative disease. Curr Opin Genet Dev *44*, 1-8.

Shorter, J., and Lindquist, S. (2004). Hsp104 catalyzes formation and elimination of self-replicating Sup35 prion conformers. Science *304*, 1793-1797.

Shorter, J., and Lindquist, S. (2006). Destruction or potentiation of different prions catalyzed by similar Hsp104 remodeling activities. Mol Cell *23*, 425-438.

bioRxiv preprint doi: https://doi.org/10.1101/2020.01.17.911016; this version posted January 18, 2020. The copyright holder for this preprint (which was not certified by peer review) is the author/funder. All rights reserved. No reuse allowed without permission.

Shorter, J., and Southworth, D.R. (2019). Spiraling in Control: Structures and Mechanisms of the Hsp104 Disaggregase. Cold Spring Harb Perspect Biol *11*.

Sirrenberg, C., Bauer, M.F., Guiard, B., Neupert, W., and Brunner, M. (1996). Import of carrier proteins into the mitochondrial inner membrane mediated by Tim22. Nature *384*, 582-585.

Spinazzi, M., Radaelli, E., Horre, K., Arranz, A.M., Gounko, N.V., Agostinis, P., Maia, T.M., Impens, F., Morais, V.A., Lopez-Lluch, G., Serneels, L., Navas, P., and De Strooper, B. (2019). PARL deficiency in mouse causes Complex III defects, coenzyme Q depletion, and Leigh-like syndrome. Proc Natl Acad Sci U S A *116*, 277-286.

Sweeny, E.A., Jackrel, M.E., Go, M.S., Sochor, M.A., Razzo, B.M., DeSantis, M.E., Gupta, K., and Shorter, J. (2015). The Hsp104 N-terminal domain enables disaggregase plasticity and potentiation. Mol Cell *57*, 836-849.

Sweeny, E.A., Tariq, A., Gurpinar, E., Go, M.S., Sochor, M.A., Kan, Z.Y., Mayne, L., Englander, S.W., and Shorter, J. (2019). Structural and mechanistic insights into Hsp104 function revealed by synchrotron x-ray footprinting. J Biol Chem.

Szklarczyk, R., Wanschers, B.F., Nabuurs, S.B., Nouws, J., Nijtmans, L.G., and Huynen, M.A. (2011). NDUFB7 and NDUFA8 are located at the intermembrane surface of complex I. FEBS Lett *585*, 737-743.

Tariq, A., Lin, J., Jackrel, M.E., Hesketh, C.D., Carman, P.J., Mack, K.L., Weitzman, R., Gambogi, C., Hernandez Murillo, O.A., Sweeny, E.A., Gurpinar, E., Yokom, A.L., Gates, S.N., Yee, K., Sudesh, S., Stillman, J., Rizo, A.N., Southworth, D.R., and Shorter, J. (2019). Mining Disaggregase Sequence Space to Safely Counter TDP-43, FUS, and alpha-Synuclein Proteotoxicity. Cell Rep *28*, 2080-2095 e2086.

Tariq, A., Lin, J., Noll, M.M., Torrente, M.P., Mack, K.L., Murillo, O.H., Jackrel, M.E., and Shorter, J. (2018). Potentiating Hsp104 activity via phosphomimetic mutations in the middle domain. FEMS Yeast Res *18*.

The Gene Ontology, C. (2019). The Gene Ontology Resource: 20 years and still GOing strong. Nucleic Acids Res *47*, D330-D338.

Tkach, J.M., and Glover, J.R. (2008). Nucleocytoplasmic trafficking of the molecular chaperone Hsp104 in unstressed and heat-shocked cells. Traffic *9*, 39-56.

Torrente, M.P., Chuang, E., Noll, M.M., Jackrel, M.E., Go, M.S., and Shorter, J. (2016). Mechanistic Insights into Hsp104 Potentiation. J Biol Chem *291*, 5101-5115.

Tzagoloff, A., Capitanio, N., Nobrega, M.P., and Gatti, D. (1990). Cytochrome oxidase assembly in yeast requires the product of COX11, a homolog of the P. denitrificans protein encoded by ORF3. EMBO J *9*, 2759-2764.

bioRxiv preprint doi: https://doi.org/10.1101/2020.01.17.911016; this version posted January 18, 2020. The copyright holder for this preprint (which was not certified by peer review) is the author/funder. All rights reserved. No reuse allowed without permission.

Vacher, C., Garcia-Oroz, L., and Rubinsztein, D.C. (2005). Overexpression of yeast Hsp104 reduces polyglutamine aggregation and prolongs survival of a transgenic mouse model of Huntington's disease. Hum Mol Genet *14*, 3425-3433.

von Janowsky, B., Major, T., Knapp, K., and Voos, W. (2006). The disaggregation activity of the mitochondrial ClpB homolog Hsp78 maintains Hsp70 function during heat stress. J Mol Biol *357*, 793-807.

Voos, W., and Rottgers, K. (2002). Molecular chaperones as essential mediators of mitochondrial biogenesis. Biochim Biophys Acta *1592*, 51-62.

Wallace, E.W., Kear-Scott, J.L., Pilipenko, E.V., Schwartz, M.H., Laskowski, P.R., Rojek, A.E., Katanski, C.D., Riback, J.A., Dion, M.F., Franks, A.M., Airoldi, E.M., Pan, T., Budnik, B.A., and Drummond, D.A. (2015). Reversible, Specific, Active Aggregates of Endogenous Proteins Assemble upon Heat Stress. Cell *162*, 1286-1298.

Wilkening, A., Rub, C., Sylvester, M., and Voos, W. (2018). Analysis of heat-induced protein aggregation in human mitochondria. J Biol Chem *293*, 11537-11552.

Wilkins, M.R., Gasteiger, E., Bairoch, A., Sanchez, J.C., Williams, K.L., Appel, R.D., and Hochstrasser, D.F. (1999). Protein identification and analysis tools in the ExPASy server. Methods Mol Biol *112*, 531-552.

Wortmann, S.B., Wevers, R.A., and de Brouwer, A.P.M. (2016). CLPB Deficiency. In GeneReviews((R)), M.P. Adam, H.H. Ardinger, R.A. Pagon, S.E. Wallace, L.J.H. Bean, K. Stephens, and A. Amemiya, eds. (Seattle (WA): University of Washington, Seattle).

Wortmann, S.B., Zietkiewicz, S., Kousi, M., Szklarczyk, R., Haack, T.B., Gersting, S.W., Muntau, A.C., Rakovic, A., Renkema, G.H., Rodenburg, R.J., Strom, T.M., Meitinger, T., Rubio-Gozalbo, M.E., Chrusciel, E., Distelmaier, F., Golzio, C., Jansen, J.H., van Karnebeek, C., Lillquist, Y., Lucke, T., Ounap, K., Zordania, R., Yaplito-Lee, J., van Bokhoven, H., Spelbrink, J.N., Vaz, F.M., Pras-Raves, M., Ploski, R., Pronicka, E., Klein, C., Willemsen, M.A., de Brouwer, A.P., Prokisch, H., Katsanis, N., and Wevers, R.A. (2015). CLPB mutations cause 3-methylglutaconic aciduria, progressive brain atrophy, intellectual disability, congenital neutropenia, cataracts, movement disorder. Am J Hum Genet *96*, 245-257.

Yamamoto, H., Esaki, M., Kanamori, T., Tamura, Y., Nishikawa, S., and Endo, T. (2002). Tim50 is a subunit of the TIM23 complex that links protein translocation across the outer and inner mitochondrial membranes. Cell *111*, 519-528.

Yoshizawa, T., Ali, R., Jiou, J., Fung, H.Y.J., Burke, K.A., Kim, S.J., Lin, Y., Peeples, W.B., Saltzberg, D., Soniat, M., Baumhardt, J.M., Oldenbourg, R., Sali, A., Fawzi, N.L., Rosen, M.K., and Chook, Y.M. (2018). Nuclear Import Receptor Inhibits Phase Separation of FUS through Binding to Multiple Sites. Cell *173*, 693-705 e622.

bioRxiv preprint doi: https://doi.org/10.1101/2020.01.17.911016; this version posted January 18, 2020. The copyright holder for this preprint (which was not certified by peer review) is the author/funder. All rights reserved. No reuse allowed without permission.

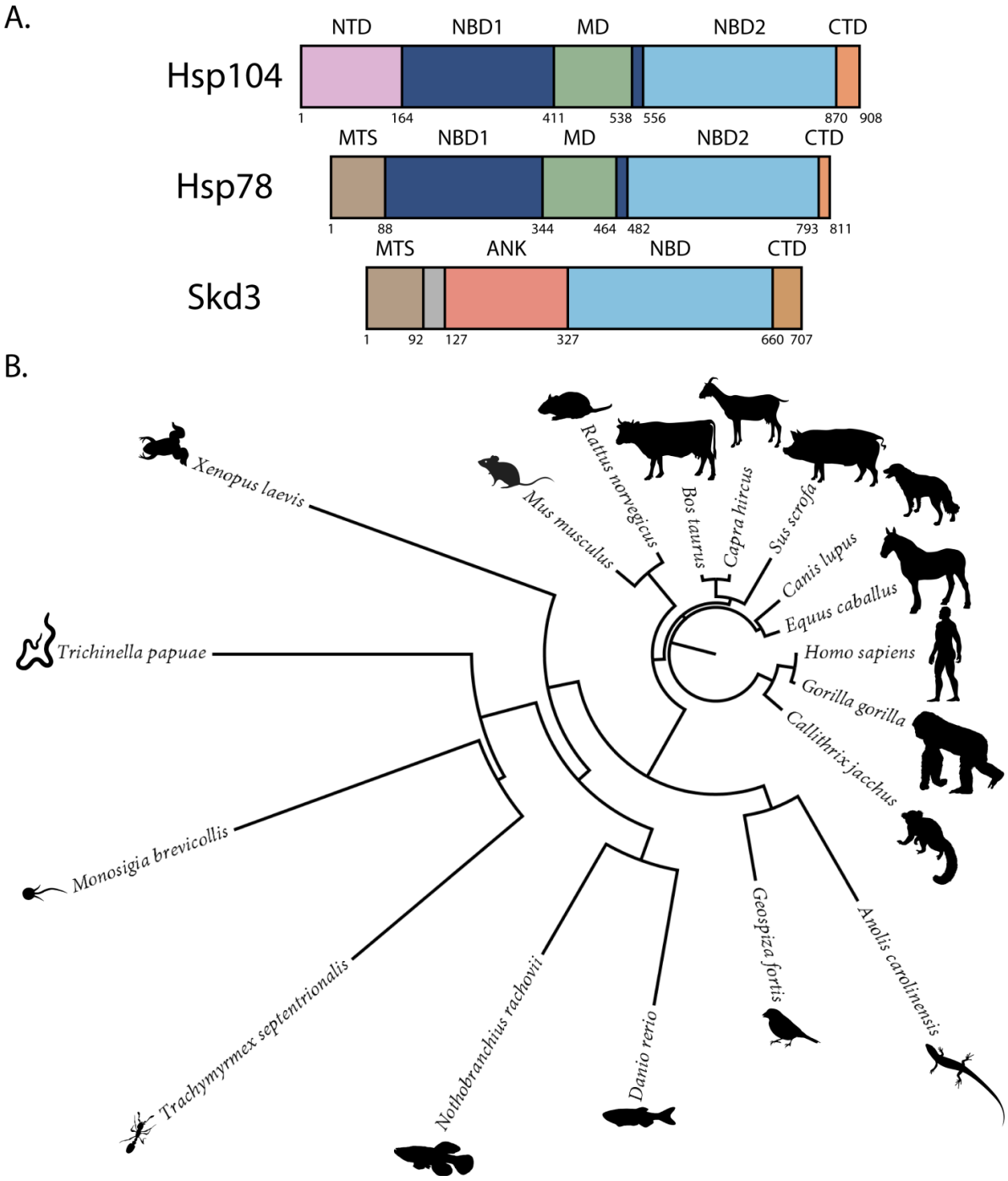

Figure 1. Skd3 is homologous to Hsp104 and Hsp78 and is conserved across diverse metazoan lineages. (A) Domain map depicting *S. cerevisiae* Hsp104, *S. cerevisiae* Hsp78, and *H. sapiens* Skd3. Hsp104 is composed of a N-terminal domain (NTD), nucleotide-binding domain 1 (NBD1), middle domain (MD), nucleotide-binding domain 2 (NBD2), and C-terminal domain (CTD). Hsp78 is composed of a mitochondrial-targeting signal (MTS), NBD1, MD, NBD2, and CTD. Skd3 is composed of a MTS, a hydrophobic domain of unknown function, an ankyrin-repeat domain (ANK) containing four ankyrin repeats, an NBD that is homologous to Hsp104 and Hsp78 NBD2, and a CTD. **(B)** Phylogenetic tree depicting a Clustal Omega alignment of Skd3 sequences from divergent metazoan lineages. The alignment shows conservation of Skd3 across diverse species and shows high similarity between mammalian Skd3 proteins.

bioRxiv preprint doi: https://doi.org/10.1101/2020.01.17.911016; this version posted January 18, 2020. The copyright holder for this preprint (which was not certified by peer review) is the author/funder. All rights reserved. No reuse allowed without permission.

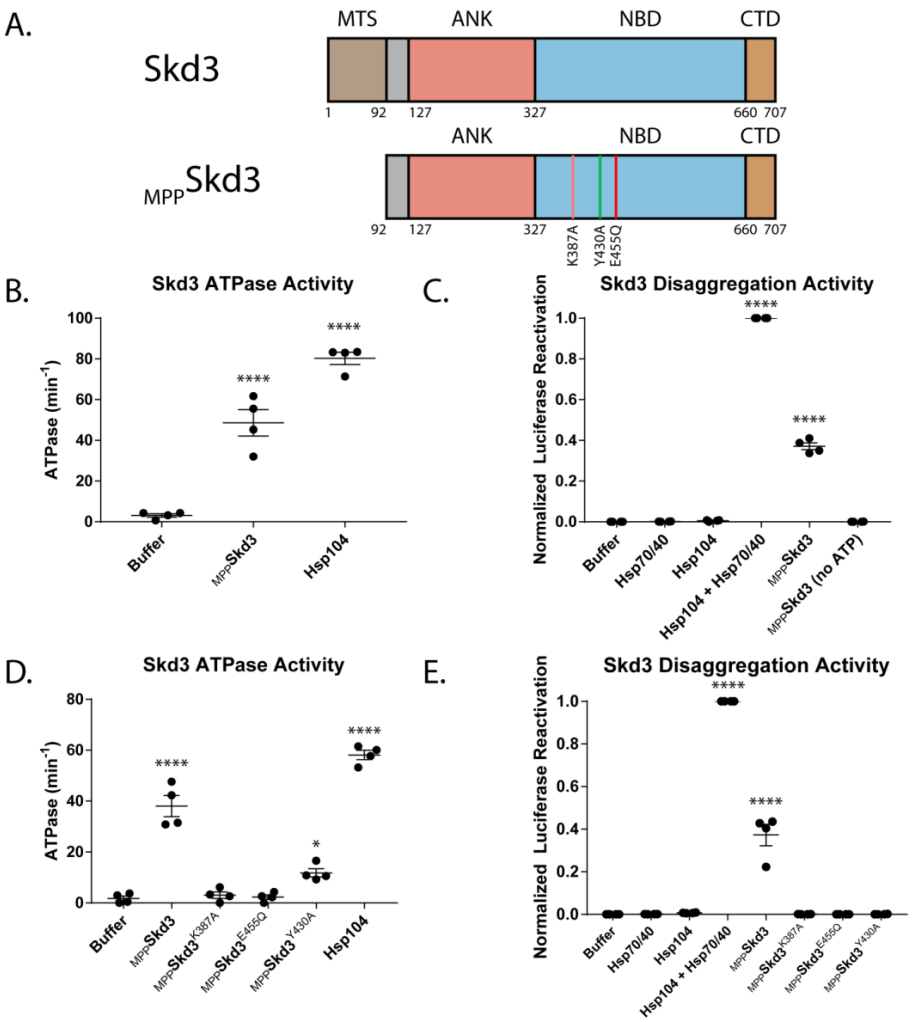

Figure 2. Skd3 is a protein disaggregase. (A) Domain map depicting the Mitochondrial-processing peptidase (MPP) cleavage site and mature-length Skd3 ($_{MPP}$Skd3). The positions of the Walker A mutation (K387A) predicted to disrupt ATP binding and hydrolysis, pore-loop tyrosine mutation (Y430A) predicted to disrupt substrate binding, and Walker B mutation (E455Q) predicted to disrupt ATP hydrolysis are shown. **(B)** $_{MPP}$Skd3 is an ATPase. ATPase assay comparing $_{MPP}$Skd3 and Hsp104. $_{MPP}$Skd3 and Hsp104 ATPase were compared to buffer using one-way ANOVA and a Dunnett's multiple comparisons test (N=4, individual data points shown as dots, bars show mean ± SEM, **** $p<0.0001$). **(C)** Luciferase disaggregation/reactivation assay showing that $_{MPP}$Skd3 has disaggregase activity in the presence but not absence of ATP. Luciferase activity was buffer subtracted and normalized to Hsp104 + Hsp70/Hsp40. Luciferase activity was compared to buffer using one-way ANOVA and a Dunnett's multiple comparisons test (N=6, individual data points shown as dots, bars show mean ± SEM, **** $p<0.0001$). **(D)** ATPase assay comparing $_{MPP}$Skd3, $_{MPP}$Skd3^{K387A} (Walker A mutant), $_{MPP}$Skd3^{E455Q} (Walker B mutant), and $_{MPP}$Skd3^{Y430A} (Pore-Loop mutant), showing that both Walker A and Walker B mutations abolish Skd3 ATPase activity, whereas the Pore Loop mutation reduces ATPase activity. ATPase activity was compared to buffer using one-way ANOVA and a Dunnett's multiple comparisons test (N=4, individual data points shown as dots, bars show mean ± SEM, * $p<0.05$, **** $p<0.0001$). **(E)** Luciferase disaggregation/reactivation assay comparing $_{MPP}$Skd3 to Walker A, Walker B, and Pore-Loop variants demonstrating that ATP binding, ATP hydrolysis, and substrate binding are essential for Skd3 disaggregase activity. Luciferase activity was compared to buffer using one-way ANOVA and a Dunnett's multiple comparisons test (N=4, individual data points shown as dots, bars show mean ± SEM, **** $p<0.0001$).

bioRxiv preprint doi: https://doi.org/10.1101/2020.01.17.911016; this version posted January 18, 2020. The copyright holder for this preprint (which was not certified by peer review) is the author/funder. All rights reserved. No reuse allowed without permission.

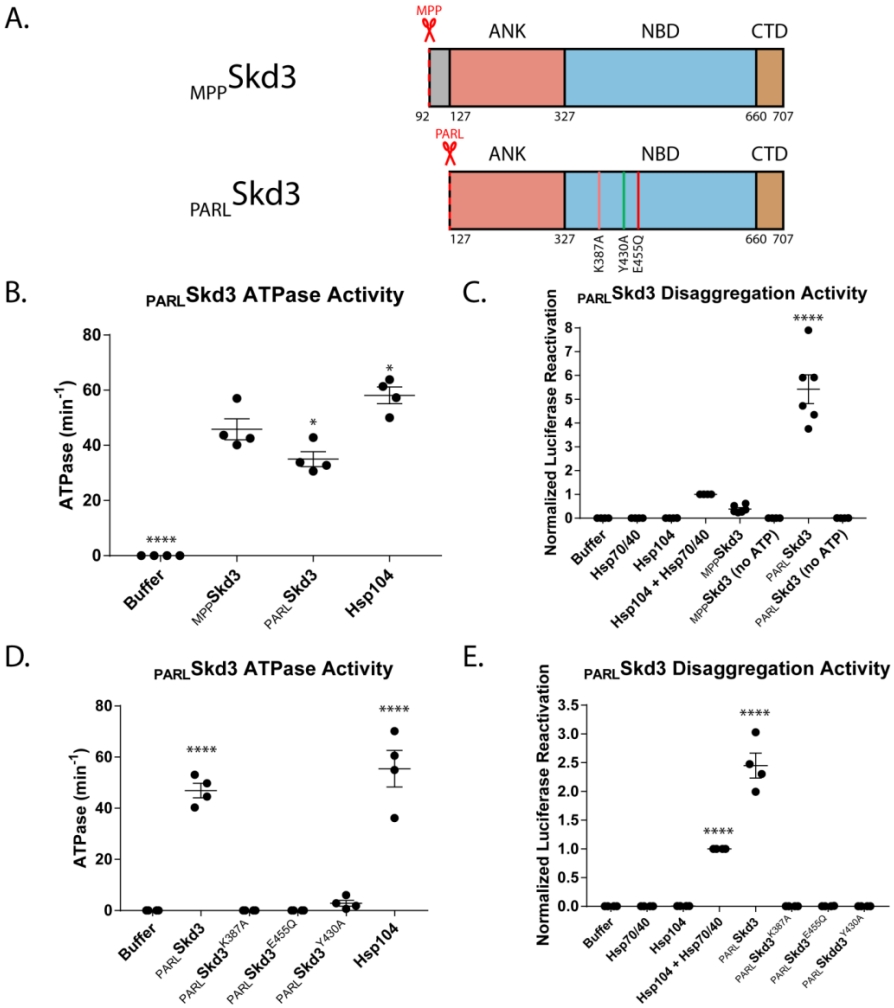

Figure 3. PARL cleavage enhances Skd3 disaggregase activity. (A) Domain map depicting $_{MPP}$Skd3 and the PARL cleavage site and corresponding PARL-cleaved Skd3 ($_{PARL}$Skd3). The positions of the Walker A mutation (K387A) predicted to disrupt ATP binding and hydrolysis, pore-loop tyrosine mutation (Y430A) predicted to disrupt substrate binding, and Walker B mutation (E455Q) predicted to disrupt ATP hydrolysis are shown. **(B)** ATPase assay comparing $_{MPP}$Skd3 and $_{PARL}$Skd3. $_{PARL}$Skd3 is catalytically active, but is slightly less active than $_{MPP}$Skd3. $_{PARL}$Skd3 and Hsp104 ATPase were compared to $_{MPP}$Skd3 ATPase using one-way ANOVA and a Dunnett's multiple comparisons test (N=4, individual data points shown as dots, bars show mean ± SEM, * $p<0.05$, **** $p<0.0001$). **(C)** Luciferase disaggregation/reactivation assay comparing $_{MPP}$Skd3 disaggregase activity to $_{PARL}$Skd3. $_{PARL}$Skd3 was over 10-fold more active than $_{MPP}$Skd3. Luciferase activity was buffer subtracted and normalized to Hsp104 + Hsp70/Hsp40. Luciferase activity was compared to $_{MPP}$Skd3 using one-way ANOVA and a Dunnett's multiple comparisons test (N=4, individual data points shown as dots, bars show mean ± SEM, **** $p<0.0001$). **(D)** ATPase assay comparing $_{PARL}$Skd3, $_{PARL}$Skd3^{K387A} (Walker A), $_{PARL}$Skd3^{E455Q} (Walker B), and $_{PARL}$Skd3^{Y430A} (Pore Loop), showing that both Walker A and Walker B mutations abolish Skd3 ATPase activity, whereas the Pore-Loop mutation reduces ATPase activity. ATPase activity was compared to buffer using one-way ANOVA and a Dunnett's multiple comparisons test (N=4, individual data points shown as dots, bars show mean ± SEM, **** $p<0.0001$). **(E)** Luciferase disaggregation/reactivation assay comparing $_{PARL}$Skd3 to Walker A, Walker B, and Pore-Loop variants showing that ATP binding, ATP hydrolysis, and substrate binding are essential for $_{PARL}$Skd3 disaggregase activity. Luciferase activity was compared to buffer using one-way ANOVA and a Dunnett's multiple comparisons test (N=4, individual data points shown as dots, bars show mean ± SEM, **** $p<0.0001$).

bioRxiv preprint doi: https://doi.org/10.1101/2020.01.17.911016; this version posted January 18, 2020. The copyright holder for this preprint (which was not certified by peer review) is the author/funder. All rights reserved. No reuse allowed without permission.

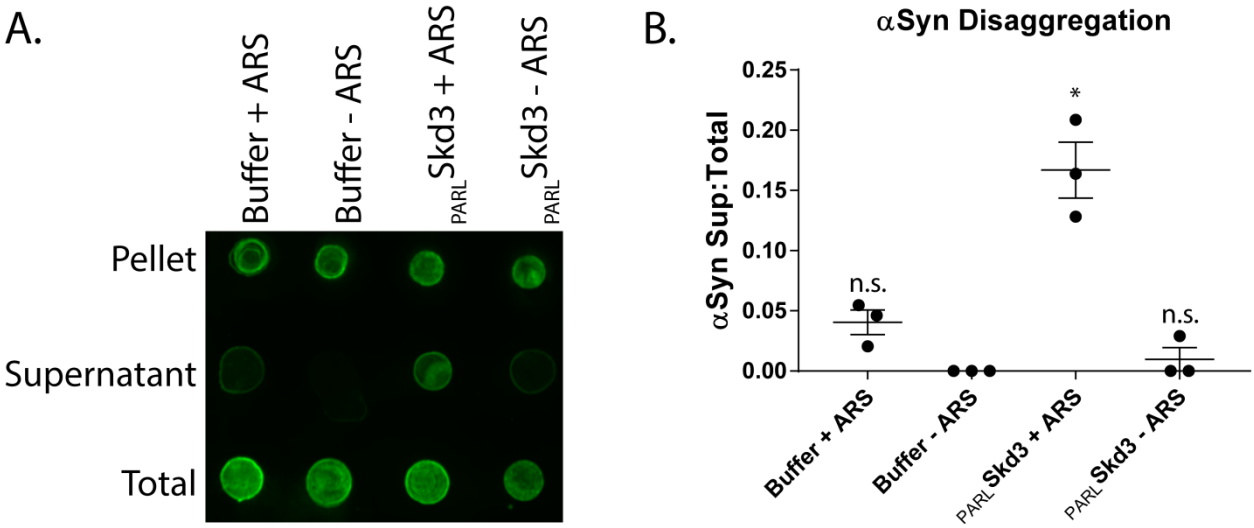

Figure 4. Skd3 disaggregates α-synuclein fibrils. (A) Representative dot blot of α-synuclein disaggregation assay. Blot shows solubilization of α-synuclein fibrils by $_{PARL}$Skd3 in the presence of an ATP regeneration system (ARS), but not in the presence of $_{PARL}$Skd3 or ARS alone. (N=3). **(B)** Quantification of α-synuclein disaggregation assay showing that $_{PARL}$Skd3 in the presence of an ARS disaggregates α-synuclein fibrils. Results are normalized as fraction in the supernatant relative to the fraction in the supernatant and the pellet. The fraction of α-synuclein in the supernatant was compared to buffer using a repeated measure one-way ANOVA and a Dunnett's multiple comparisons test (N=3, individual data points shown as dots, bars show mean ± SEM, * $p<0.05$).

bioRxiv preprint doi: https://doi.org/10.1101/2020.01.17.911016; this version posted January 18, 2020. The copyright holder for this preprint (which was not certified by peer review) is the author/funder. All rights reserved. No reuse allowed without permission.

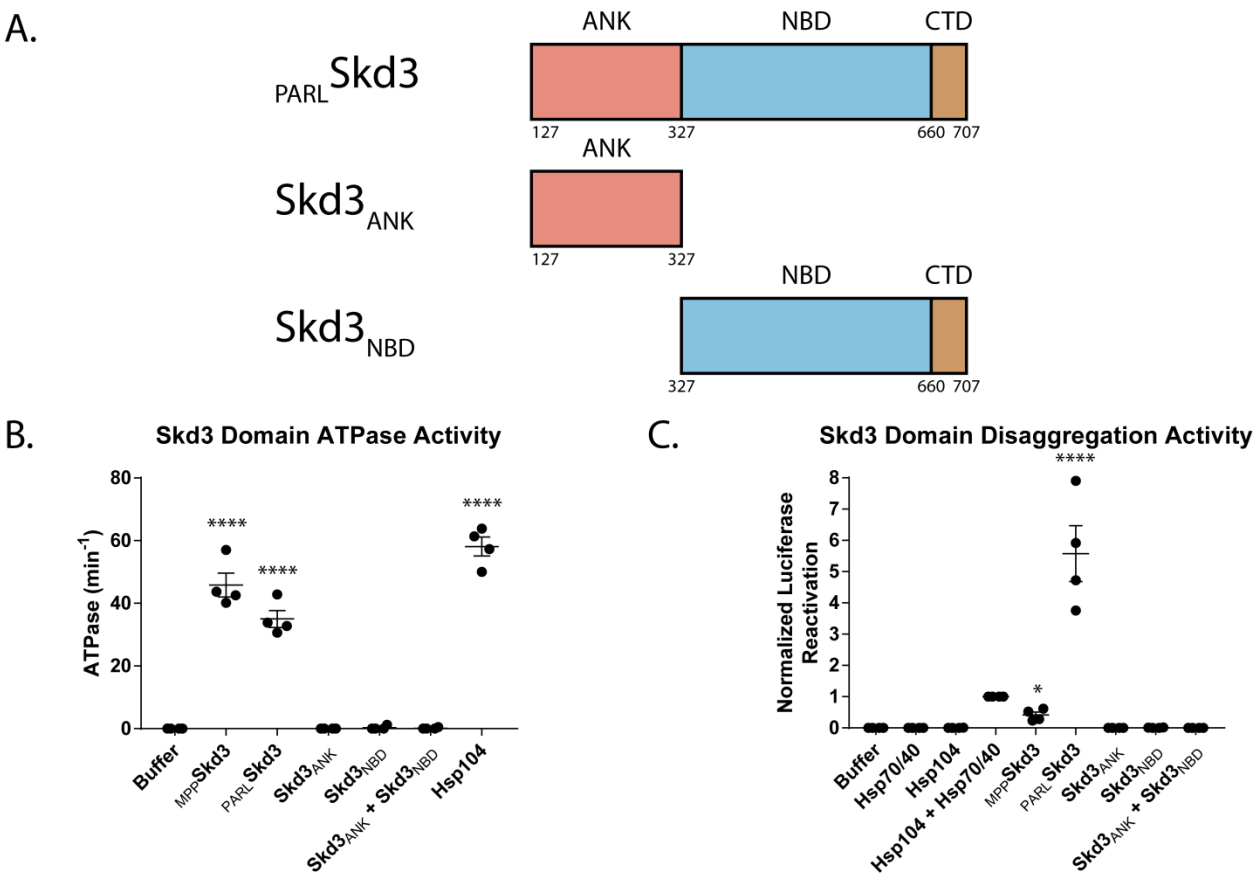

Figure 5. The ankyrin-repeat domain and NBD are required for Skd3 disaggregase activity. (A) Domain maps showing the $_{ANK}$Skd3 and $_{NBD}$Skd3 constructs. **(B)** ATPase assay comparing $_{ANK}$Skd3 and $_{NBD2}$Skd3 ATPase activity. Results show that $_{ANK}$Skd3, $_{NBD}$Skd3, and $_{ANK}$Skd3 + $_{NBD2}$Skd3 do not have ATPase activity. Data is from the same experiments as Figure 3B. ATPase activity was compared to buffer using one-way ANOVA and a Dunnett's multiple comparisons test (N=4, individual data points shown as dots, bars show mean ± SEM, **** $p<0.0001$). **(C)** Luciferase disaggregation/reactivation assay comparing $_{ANK}$Skd3, $_{NBD}$Skd3, and $_{ANK}$Skd3 + $_{NBD}$Skd3 disaggregation activity. Results show that $_{ANK}$Skd3, $_{NBD}$Skd3, or $_{ANK}$Skd3 + $_{NBD}$Skd3 are inactive disaggregases. Data is from same experiments as Figure 3C. Luciferase activity was buffer subtracted and normalized to Hsp104 plus Hsp70 and Hsp40. Luciferase disaggregase activity was compared to buffer using one-way ANOVA and a Dunnett's multiple comparisons test (N=4, individual data points shown as dots, bars show mean ± SEM, **** $p<0.0001$).

bioRxiv preprint doi: https://doi.org/10.1101/2020.01.17.911016; this version posted January 18, 2020. The copyright holder for this preprint (which was not certified by peer review) is the author/funder. All rights reserved. No reuse allowed without permission.

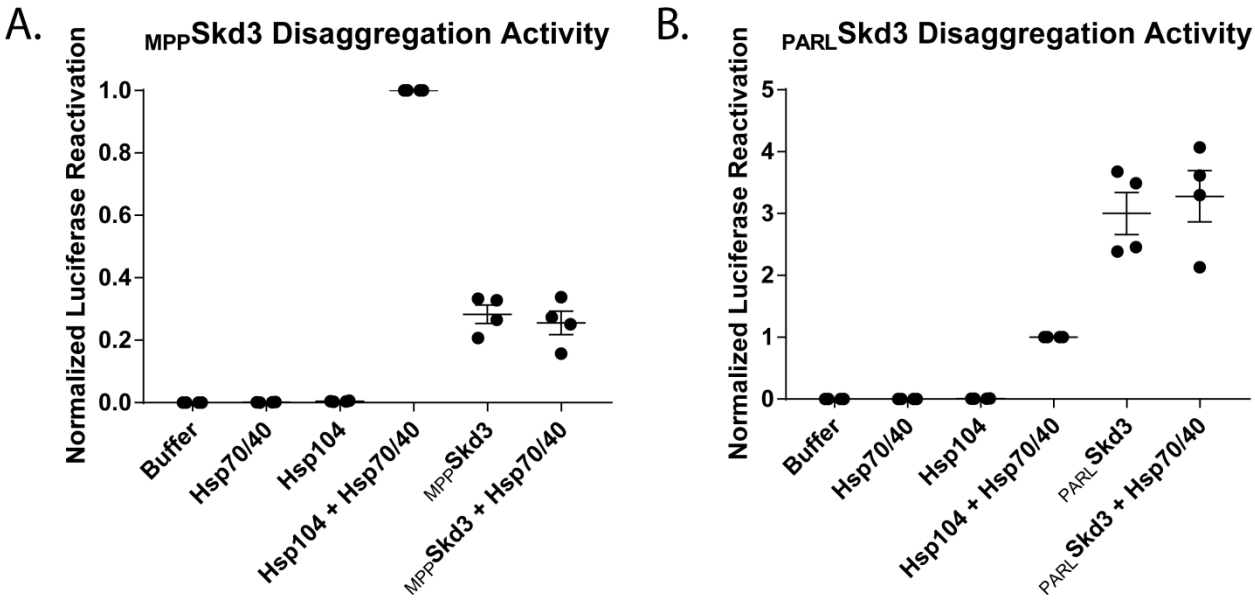

Figure 6. Skd3 does not collaborate with Hsp70 and Hsp40 in protein disaggregation. (A) Luciferase disaggregation/reactivation comparing $_{MPP}$Skd3 disaggregase activity in the presence and absence of Hsp70 (Hsc70) and Hsp40 (Hdj1). Results show a stimulation of Hsp104 disaggregase activity by Hsp70 and Hsp40, but no stimulation of disaggregase activity for $_{MPP}$Skd3. $_{MPP}$Skd3 plus Hsp70 and Hsp40 was compared to $_{MPP}$Skd3 using a two-tailed, unpaired t-test. Test found no significant difference in disaggregation activity. (N=4, individual data points shown as dots, bars show mean ± SEM). **(B)** Luciferase disaggregation/reactivation comparing $_{PARL}$Skd3 disaggregase activity in the presence and absence of Hsp70 and Hsp40. Results show no stimulation of disaggregase activity for $_{PARL}$Skd3 by Hsp70 and Hsp40. $_{PARL}$Skd3 plus Hsp70 and Hsp40 was compared to $_{PARL}$Skd3 using a two-tailed, unpaired t-test. Test found no significant difference in disaggregation activity. (N=4, individual data points shown as dots, bars show mean ± SEM).

bioRxiv preprint doi: https://doi.org/10.1101/2020.01.17.911016; this version posted January 18, 2020. The copyright holder for this preprint (which was not certified by peer review) is the author/funder. All rights reserved. No reuse allowed without permission.

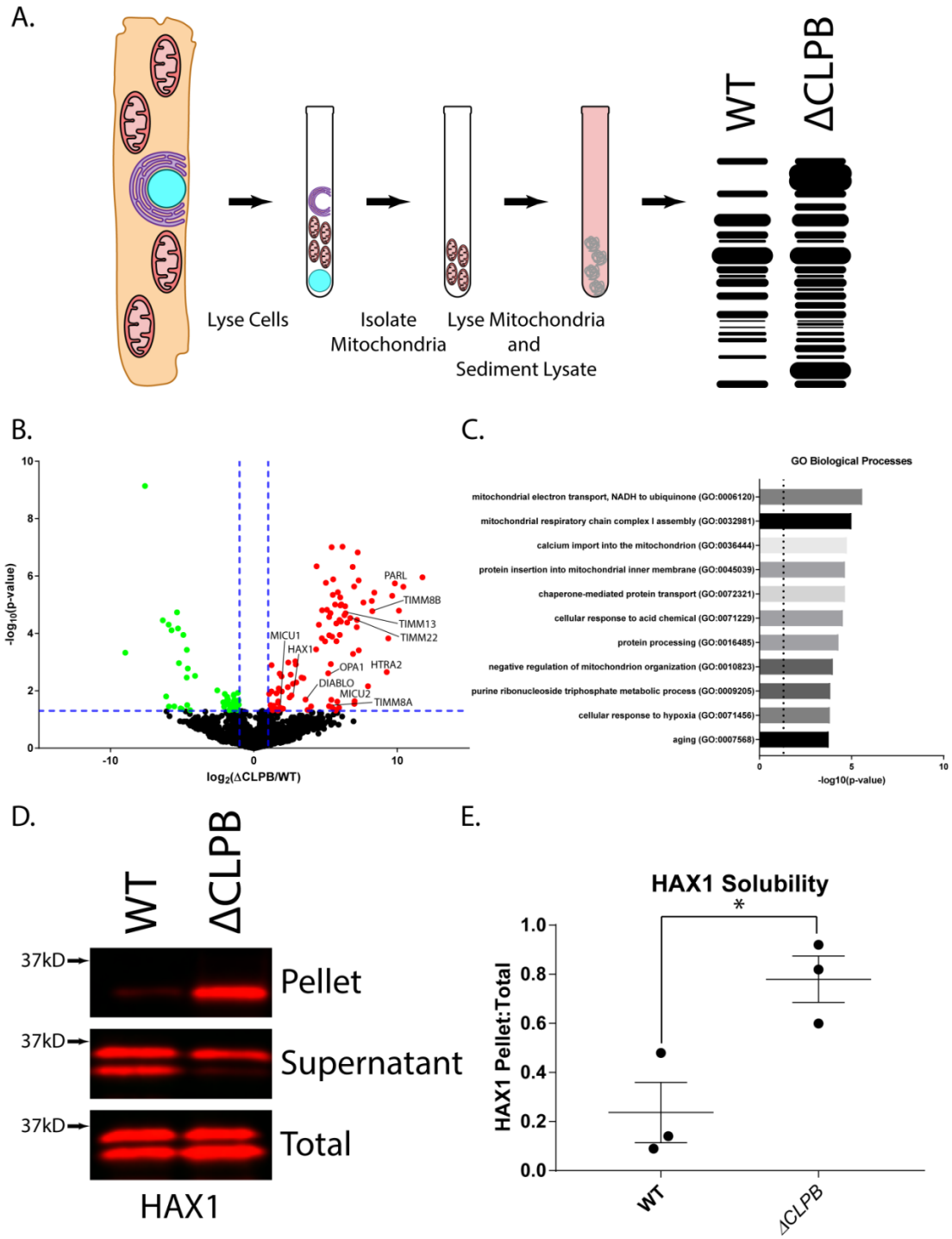

Figure 7. Skd3 maintains the solubility of key mitochondrial proteins in human cells. (A) Schematic showing sedimentation assay design. HAP1 cells were lysed and the mitochondrial fraction was separated from the cytosolic fraction. The mitochondrial fraction was then lysed and the soluble fraction was separated from the insoluble fraction via sedimentation. The samples were then either analyzed via mass-spectrometry or western blotting. **(B)** Volcano plot showing the $\log_2$ fold change of protein in the Skd3 (ClpB) knockout pellet compared to the wild-type pellet. The 99 proteins that were enriched in the Skd3 pellet are highlighted in red. The 53 proteins that were enriched in the wild-type pellet are highlighted in green. Significance cutoffs were set as fold change >2.0 and $p<0.05$, indicated with blue dashed lines

bioRxiv preprint doi: https://doi.org/10.1101/2020.01.17.911016; this version posted January 18, 2020. The copyright holder for this preprint (which was not certified by peer review) is the author/funder. All rights reserved. No reuse allowed without permission.

(N=3, $p<0.05$). **(C)** Select statistically significant terms for GO biological processes from the enriched proteins in the Skd3 knockout pellet. Dashed line shows $p=0.05$ ($p<0.05$). For full list see Fig. S9b. **(D)** Representative western blot of sedimentation assay showing relative solubility of HAX1 protein in wild-type and Skd3 (ClpB) knockout cells. Results show a marked decrease in HAX1 solubility when Skd3 is knocked out. (N=3). **(E)** Quantification of HAX1 sedimentation assay shows an overall increase in the insoluble HAX1 relative to the total protein in the Skd3 (ClpB) knockout cell line. Quantification is normalized as signal in the pellet divided by the sum of the signal in the pellet and supernatant. The fraction in the pellet for the Skd3 knockout was compared to the wild-type cells using a two-way, unpaired, t-test. (N=3, individual data points shown as dots, bars show mean ± SEM, * $p<0.05$).

bioRxiv preprint doi: https://doi.org/10.1101/2020.01.17.911016; this version posted January 18, 2020. The copyright holder for this preprint (which was not certified by peer review) is the author/funder. All rights reserved. No reuse allowed without permission.

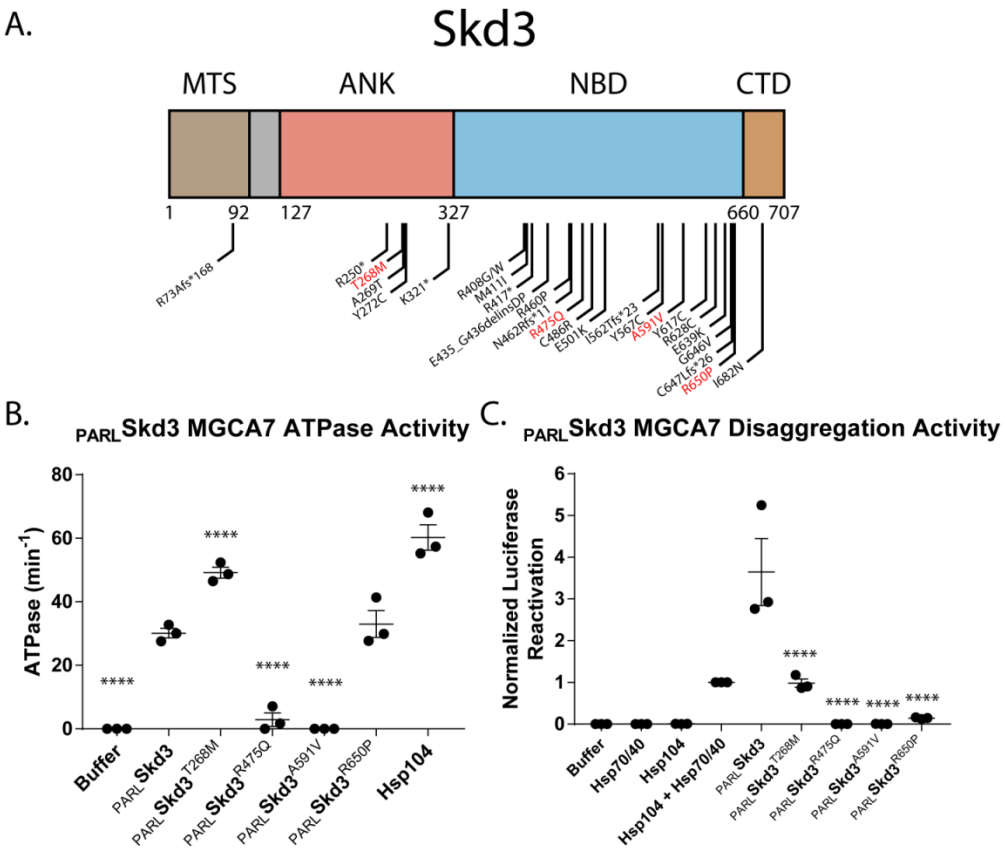

D.

	Severity	ATPase	Disaggregase
$_{PARL}$Skd3	------	1.00 +/- 0.00	1.00 +/- 0.00
$_{PARL}$Skd3^{T268M}	Moderate	1.64 +/- 0.11	0.28 +/- 0.03
$_{PARL}$Skd3^{R475Q}	Severe	0.10 +/- 0.07	0.00 +/- 0.00
$_{PARL}$Skd3^{A591V}	Severe	0.00 +/- 0.00	0.00 +/- 0.00
$_{PARL}$Skd3^{R650P}	Severe	1.11 +/- 0.19	0.04 +/- 0.01

Figure 8: Skd3 disaggregase activity predicts the clinical severity of MGCA7-associated mutations. **(A)** Domain map depicting all published mutations in Skd3 that have been associated with MGCA7. Mutants in red are studied further here. **(B)** ATPase assay showing the effect of four homozygous MGCA7 mutations on Skd3 activity. $_{PARL}$Skd3^{T268M} has increased ATPase activity, $_{PARL}$Skd3^{R475Q} and $_{PARL}$Skd3^{A591V} have decrease ATPase activity, and $_{PARL}$Skd3^{R650P} has unchanged ATPase activity compared to wild type. $_{PARL}$Skd3 MGCA7 mutants ATPase activities were compared to $_{PARL}$Skd3 wild-type using one-way ANOVA and a Dunnett's multiple comparisons test (N=3, individual data points shown as dots, bars show mean ± SEM, **** $p<0.0001$). **(C)** Luciferase disaggregation/reactivation assay showing the effect of the same four homozygous MGCA7 mutations on Skd3 activity. $_{PARL}$Skd3^{T268M} had reduced disaggregase activity, whereas $_{PARL}$Skd3^{R475Q}, $_{PARL}$Skd3^{A591V}, and $_{PARL}$Skd3^{R650P} had almost completely inactive disaggregase activity compared to wild type. Luciferase activity was buffer subtracted and normalized to Hsp104 plus Hsp70 and Hsp40. Luciferase disaggregase activity was compared to $_{PARL}$Skd3 wild type using one-way ANOVA and a Dunnett's multiple comparisons test (N=3, individual data points shown as dots, bars show mean ± SEM, **** $p<0.0001$). **(D)** Table summarizing the clinical severity of each MGCA7 mutation as well as the ATPase activity and luciferase disaggregase activity. The table shows a relationship between luciferase disaggregase activity and clinical severity, but no relationship between either the ATPase activity and clinical severity or ATPase and luciferase disaggregase activity. Values represent ATPase activity and luciferase disaggregase activity normalized to wild-type $_{PARL}$Skd3 activity. Values show mean ± SEM (N=3).

bioRxiv preprint doi: https://doi.org/10.1101/2020.01.17.911016; this version posted January 18, 2020. The copyright holder for this preprint (which was not certified by peer review) is the author/funder. All rights reserved. No reuse allowed without permission.

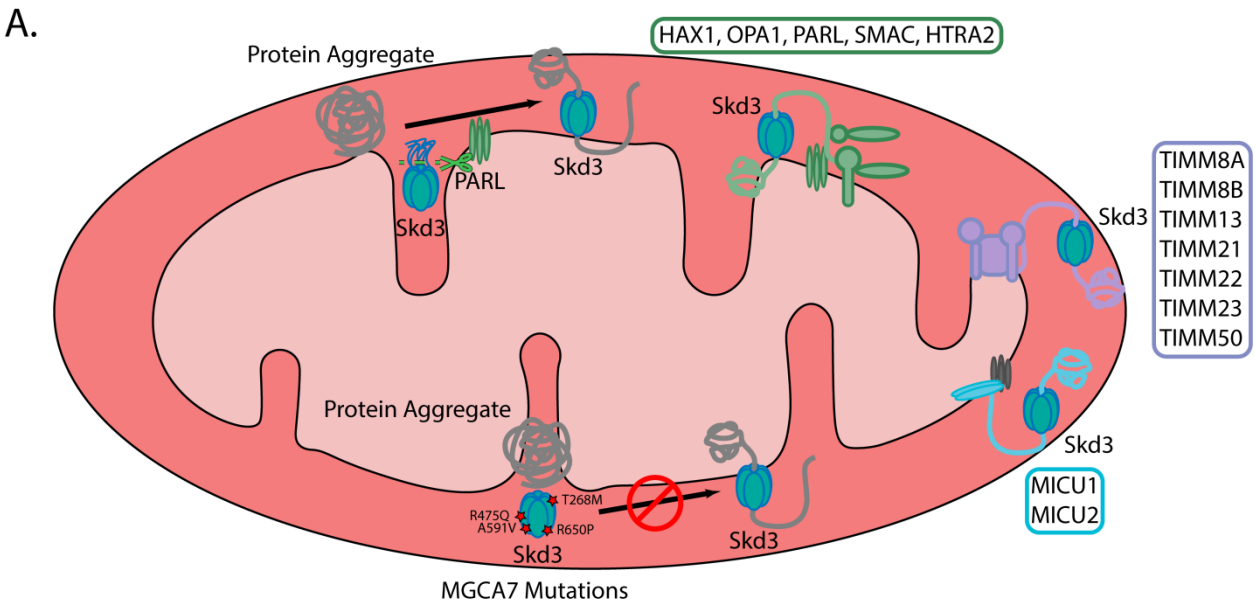

Figure 9. Skd3 is a protein disaggregase that is activated by PARL and inactivated by MGCA7-linked mutations. (A) Schematic illustrating (i) that Skd3 is a protein disaggregase that is activated by PARL cleavage of its hydrophobic auto-inhibitory domain, (ii) that Skd3 works to solubilize key substrates in the mitochondrial intermembrane space and inner membrane that are involved in apoptosis, protein import, calcium handling, and respiration, and (iii) that mutations in Skd3 associated with MGCA7 result in defective Skd3 disaggregase activity in a manner that predicts the clinical severity of disease.

bioRxiv preprint doi: https://doi.org/10.1101/2020.01.17.911016; this version posted January 18, 2020. The copyright holder for this preprint (which was not certified by peer review) is the author/funder. All rights reserved. No reuse allowed without permission.

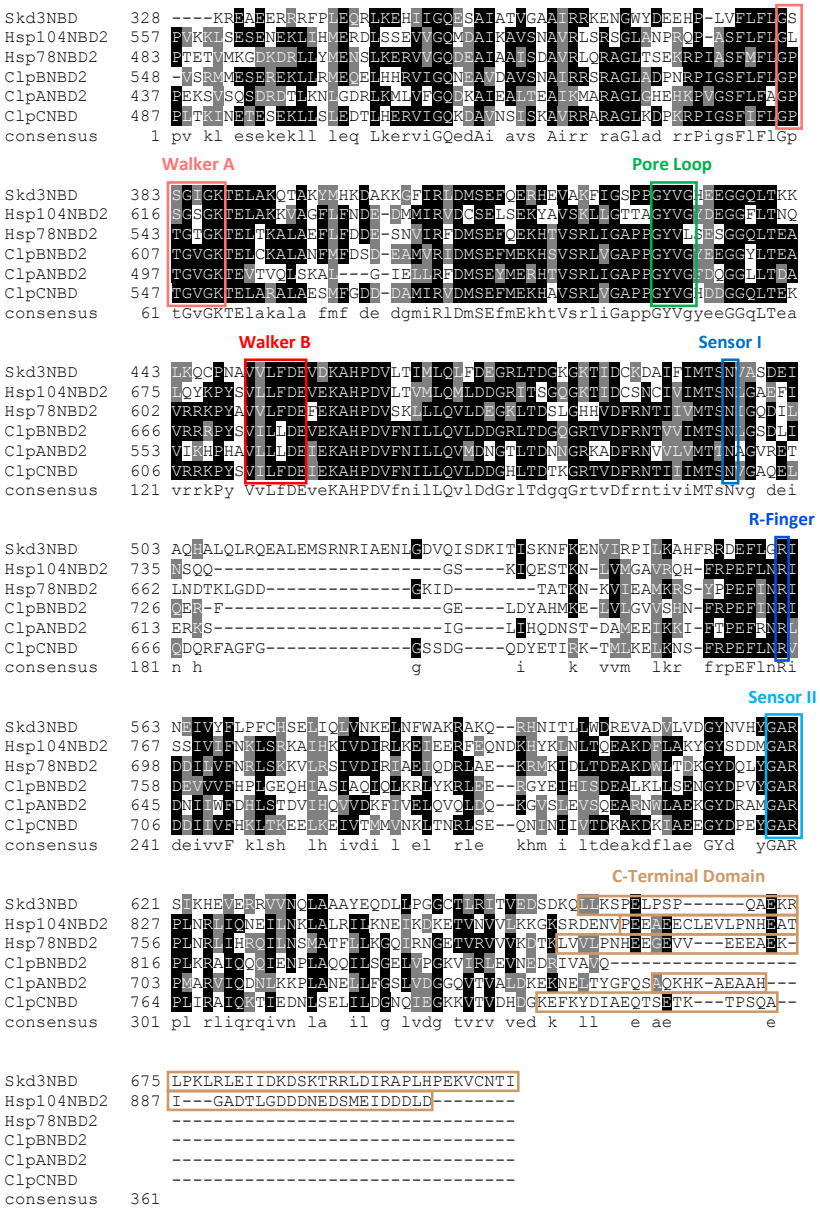

Figure S1: Skd3 NBD alignment to other AAA+ proteins reveals high similarity to Hsp104 and Hsp78. Alignment of NBD2s from *H. sapiens* Skd3, *S. cerevisiae* Hsp104, *S. cerevisiae* Hsp78, *E. coli* ClpB, *E. coli* ClpA, and *S. aureus* ClpC. Alignments were constructed using Clustal Omega. Bottom row shows consensus sequence of alignment. Highlighted in red are the Walker A and Walker B motifs. Highlighted in green are the Pore Loop motifs. Highlighted in blue are the Sensor I, Sensor II, and Arginine Finger motifs.

bioRxiv preprint doi: https://doi.org/10.1101/2020.01.17.911016; this version posted January 18, 2020. The copyright holder for this preprint (which was not certified by peer review) is the author/funder. All rights reserved. No reuse allowed without permission.

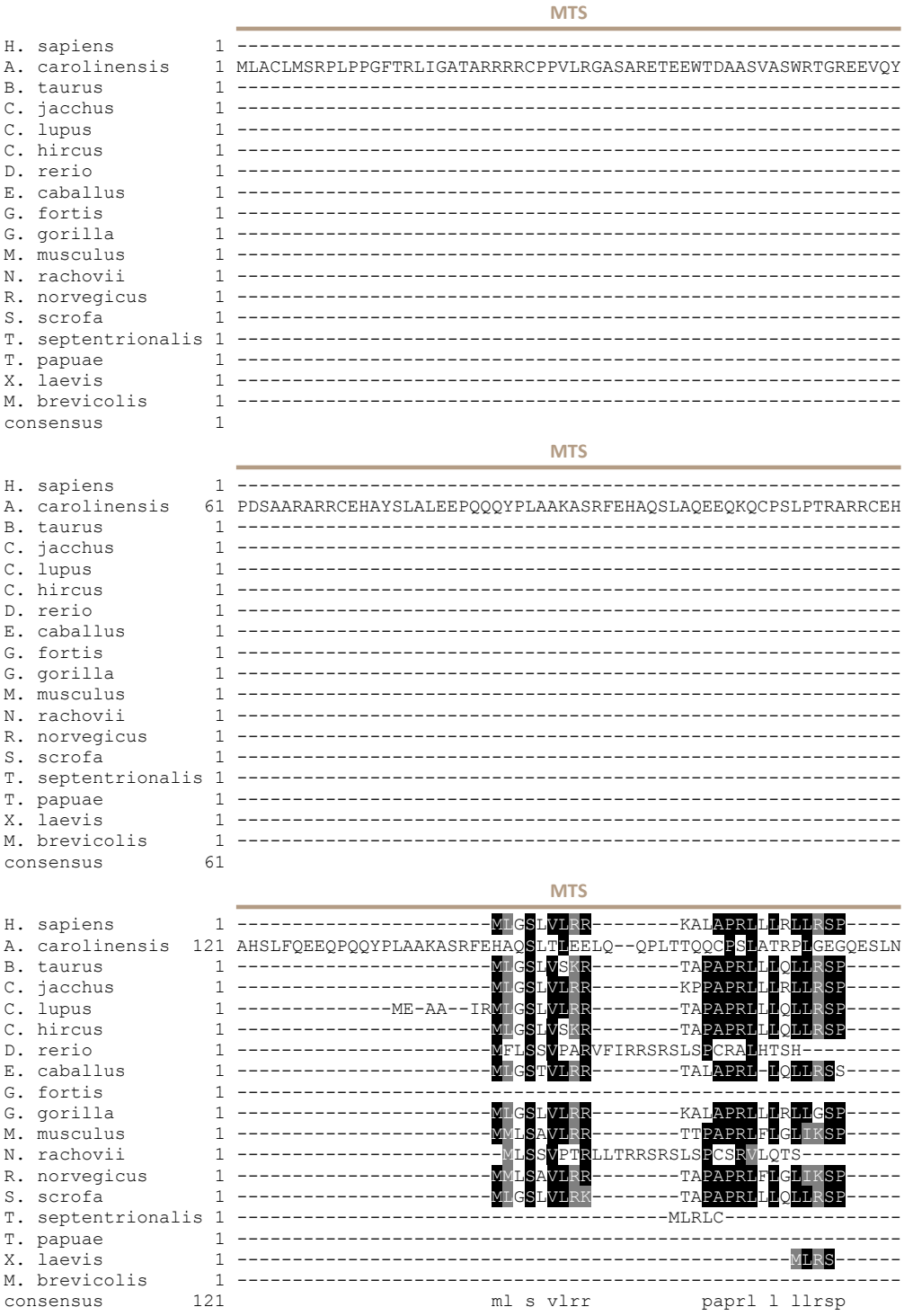

bioRxiv preprint doi: https://doi.org/10.1101/2020.01.17.911016; this version posted January 18, 2020. The copyright holder for this preprint (which was not certified by peer review) is the author/funder. All rights reserved. No reuse allowed without permission.

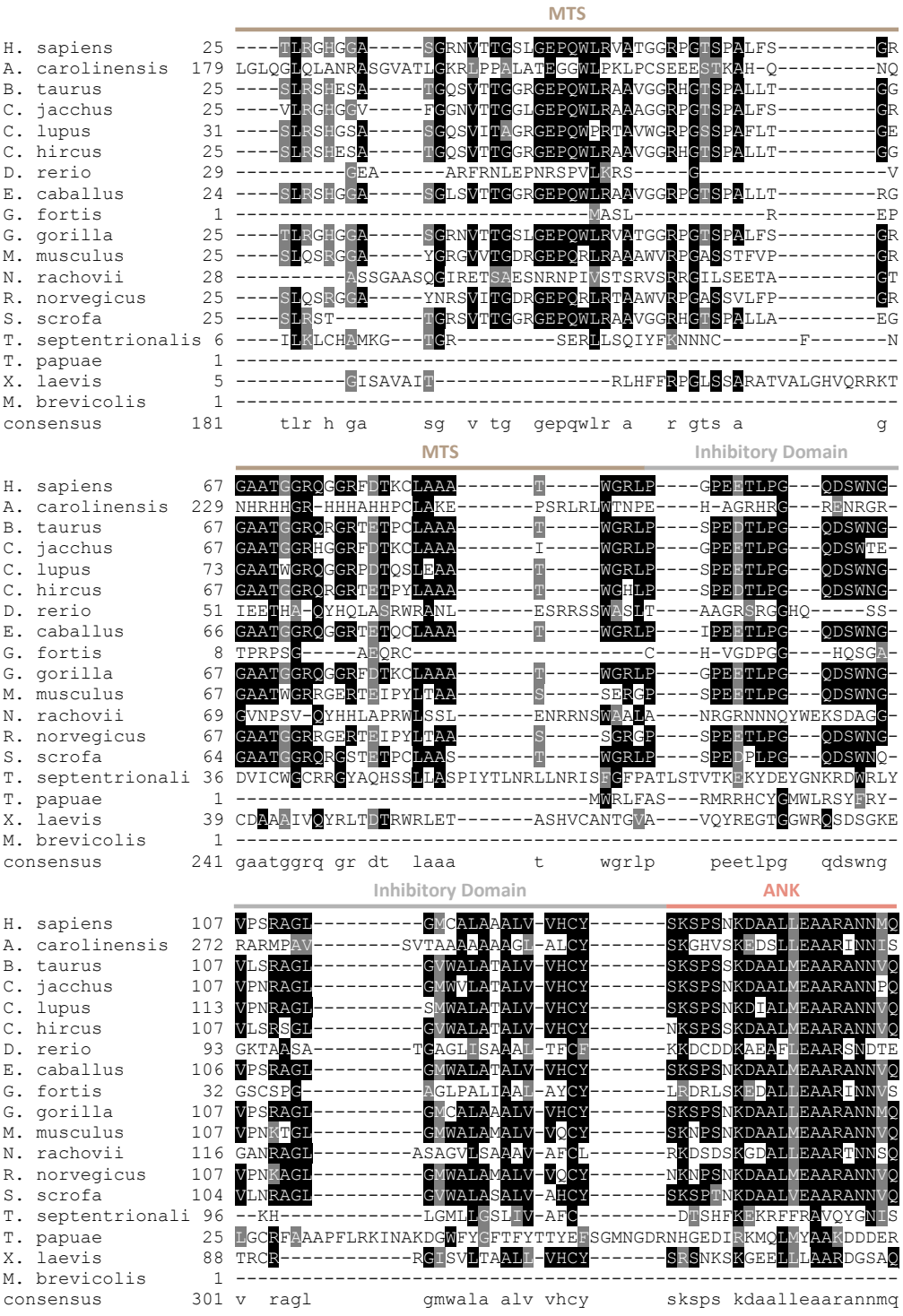

bioRxiv preprint doi: https://doi.org/10.1101/2020.01.17.911016; this version posted January 18, 2020. The copyright holder for this preprint (which was not certified by peer review) is the author/funder. All rights reserved. No reuse allowed without permission.

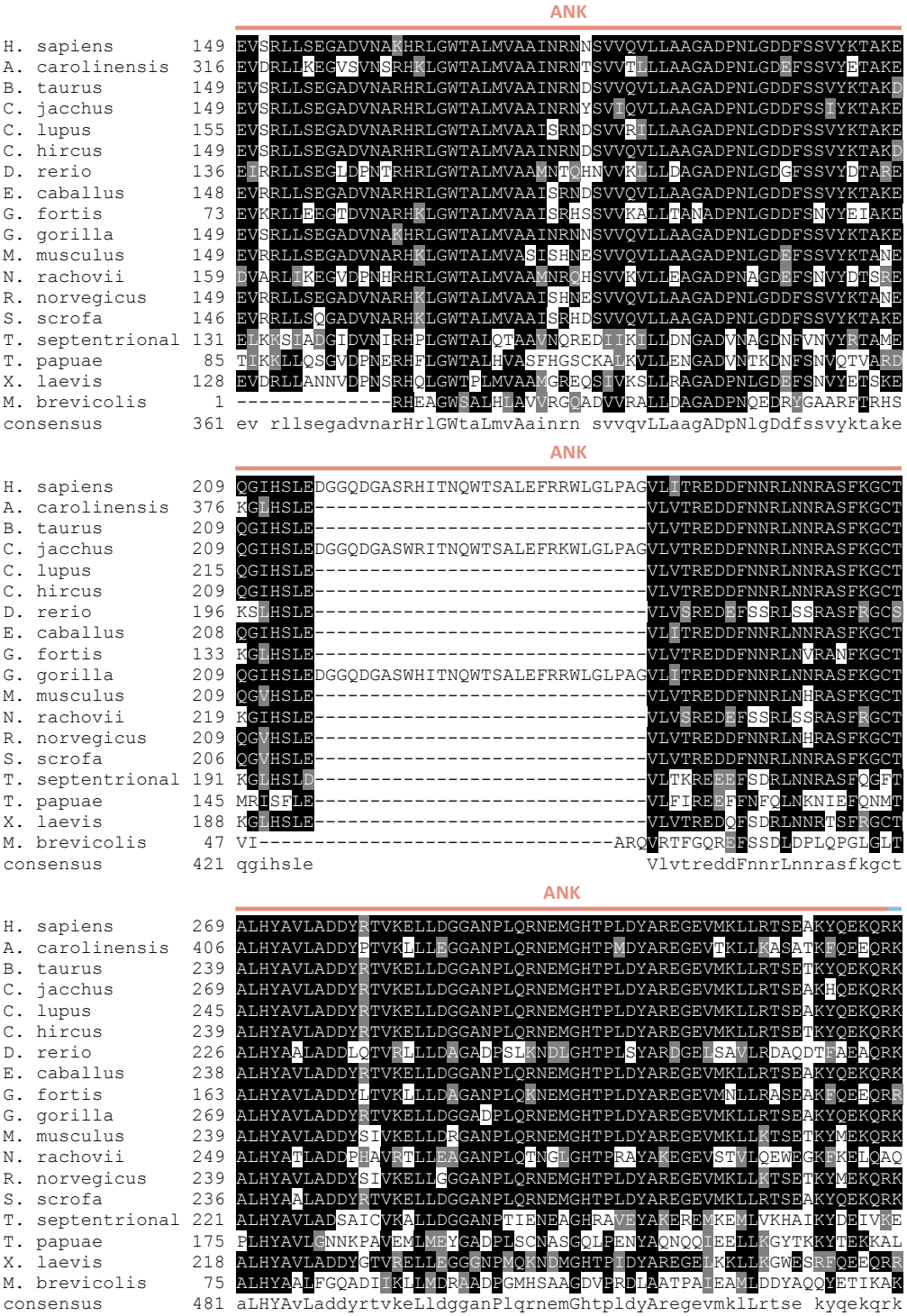

bioRxiv preprint doi: https://doi.org/10.1101/2020.01.17.911016; this version posted January 18, 2020. The copyright holder for this preprint (which was not certified by peer review) is the author/funder. All rights reserved. No reuse allowed without permission.

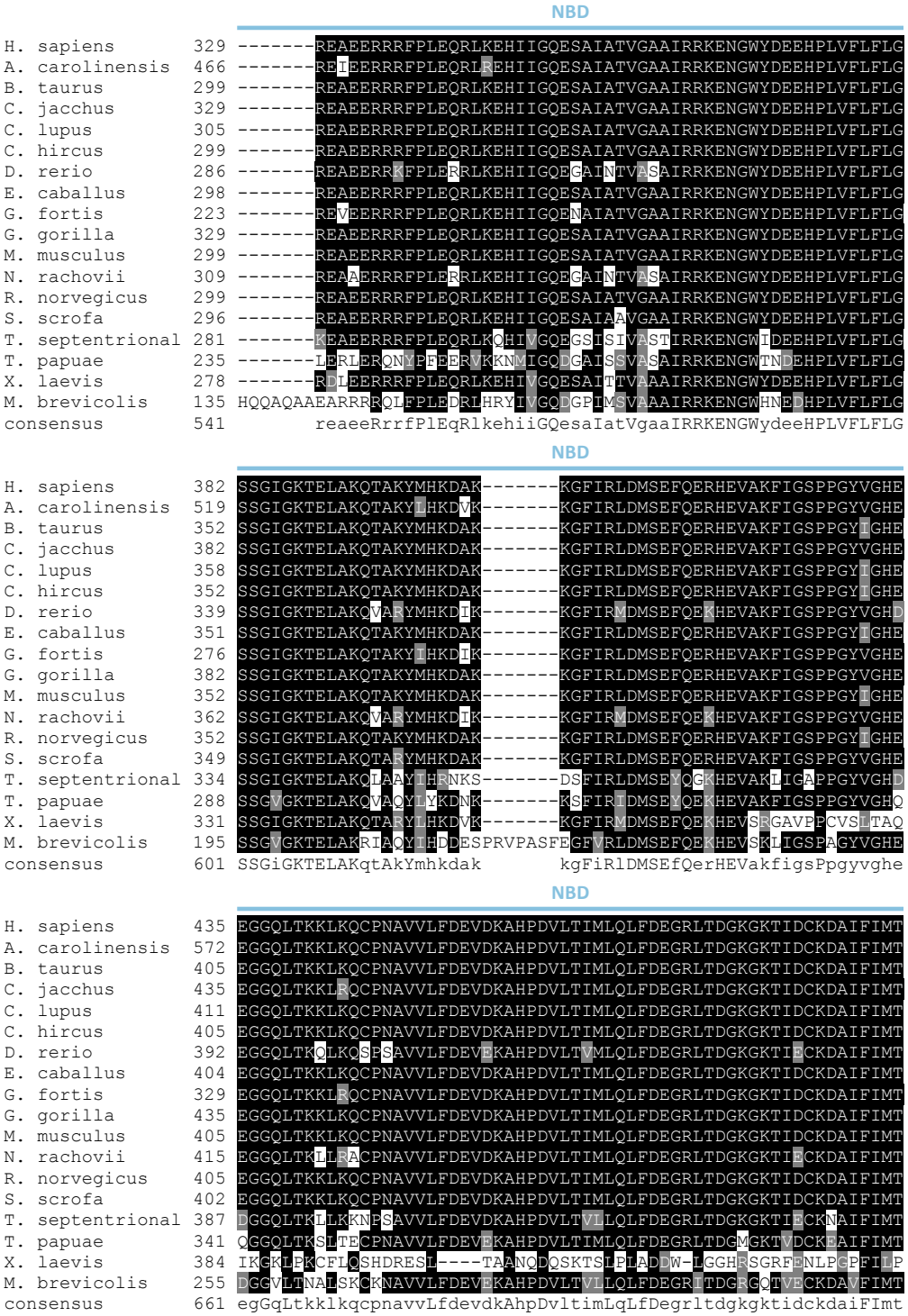

bioRxiv preprint doi: https://doi.org/10.1101/2020.01.17.911016; this version posted January 18, 2020. The copyright holder for this preprint (which was not certified by peer review) is the author/funder. All rights reserved. No reuse allowed without permission.

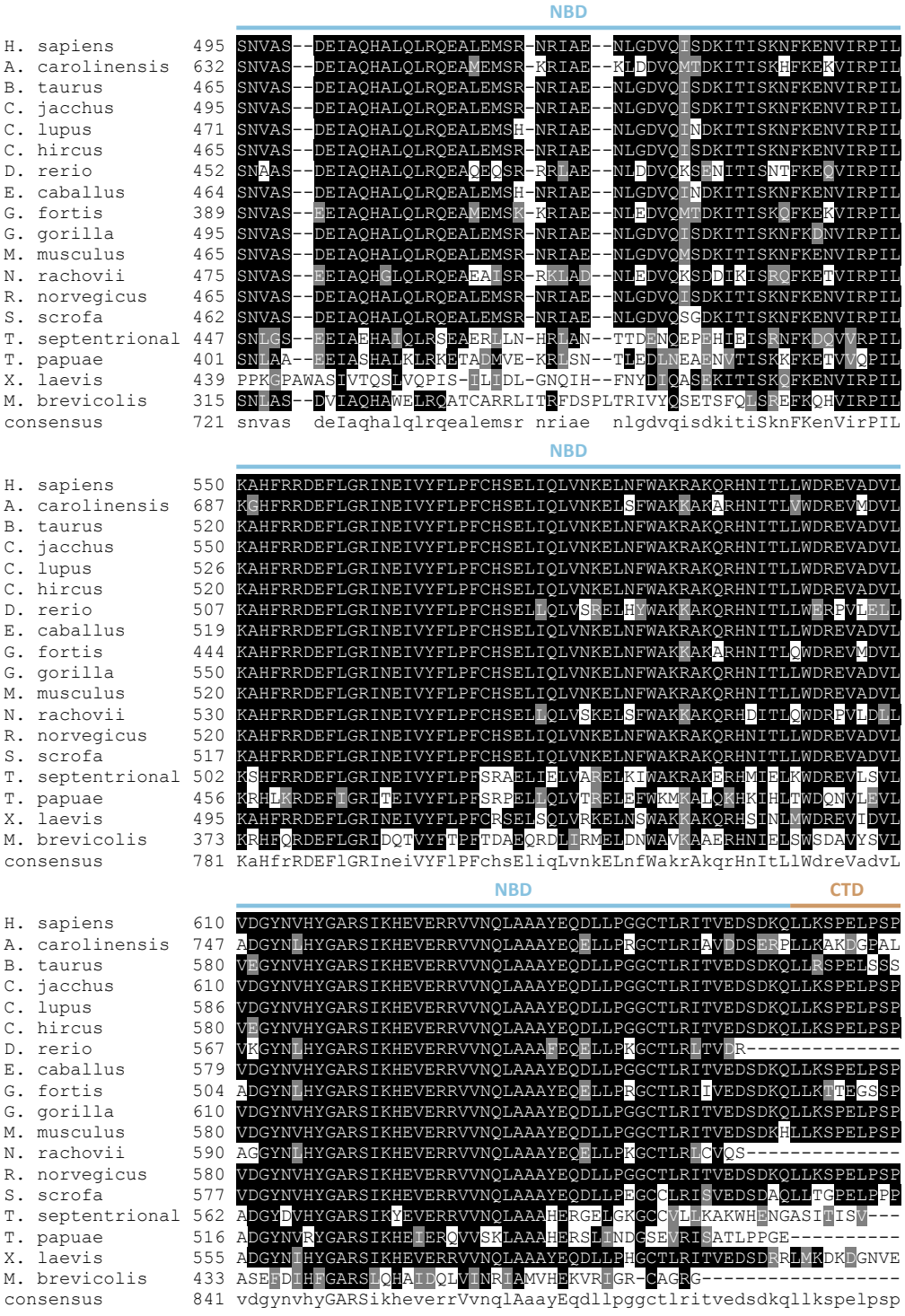

bioRxiv preprint doi: https://doi.org/10.1101/2020.01.17.911016; this version posted January 18, 2020. The copyright holder for this preprint (which was not certified by peer review) is the author/funder. All rights reserved. No reuse allowed without permission.

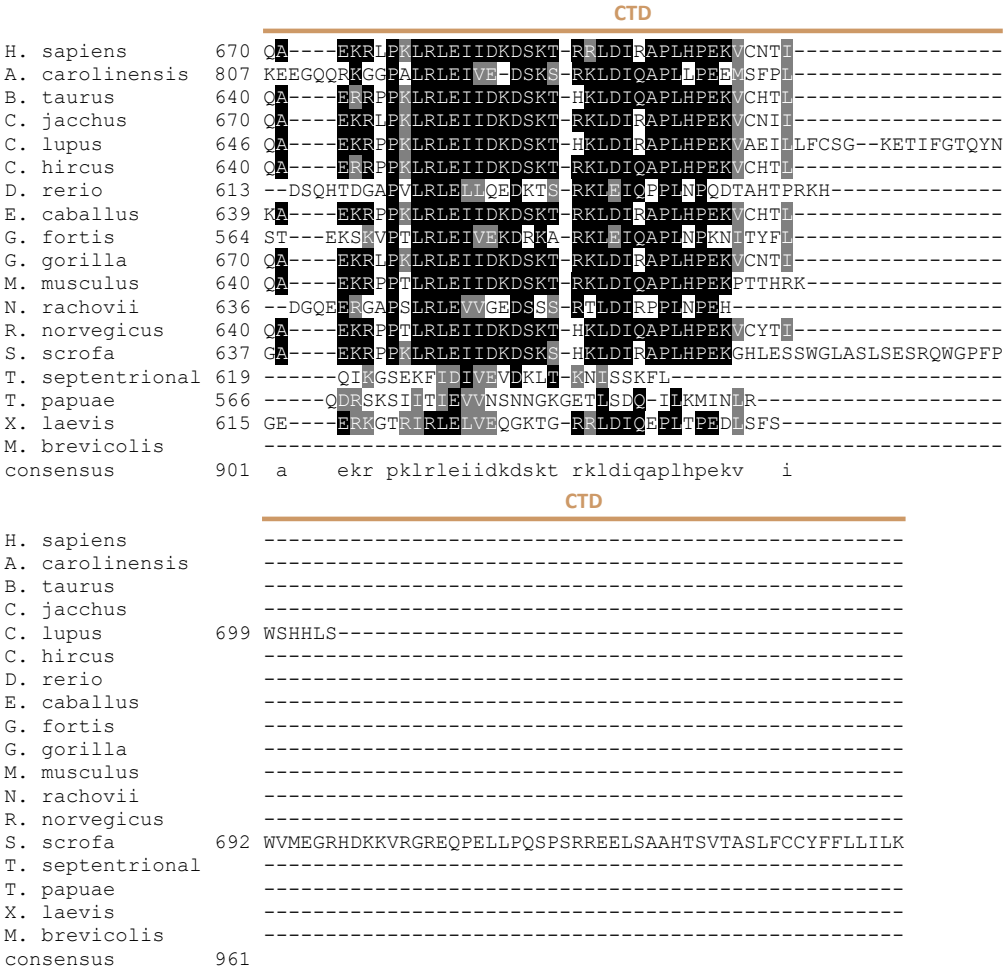

Figure S2. Alignment of Skd3 to diverse metazoan lineages shows conservation of key motifs and domains. Alignment of Skd3 protein from diverse metazoan lineages. Alignment was constructed using Clustal Omega. Alignment shows high level of conservation of Skd3 among species. *H. sapiens*, *G. gorilla*, and *C. jacchus* Skd3 have an additional insertion in the ankyrin repeat domain that is not conserved in the other species. This alignment was used to generate the phylogenetic tree in Figure 1B. The *M. brevicollis* Skd3 sequence was included in the alignment for reference. MTS (mitochondrial-targeting sequence, ANK (ankyrin-repeat domain), NBD (nucleotide-binding domain), and CTD (C-terminal domain).

bioRxiv preprint doi: https://doi.org/10.1101/2020.01.17.911016; this version posted January 18, 2020. The copyright holder for this preprint (which was not certified by peer review) is the author/funder. All rights reserved. No reuse allowed without permission.

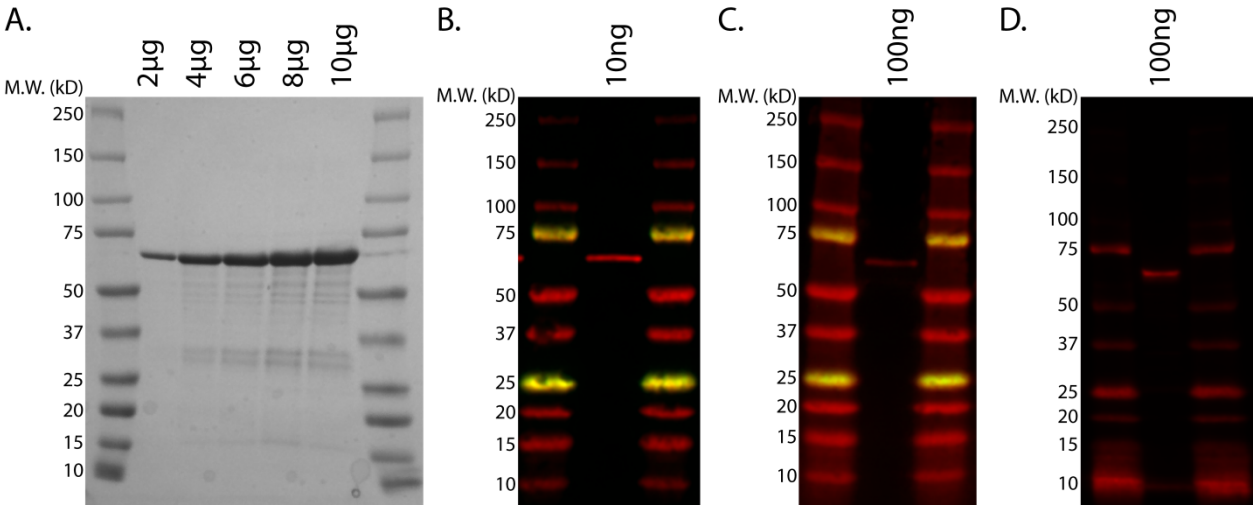

Figure S3. Recombinant Skd3 is highly pure and immunoreactive with several commercially available antibodies. (A) Representative gel of $_{MPP}$Skd3 showing high purity via Coomassie Brilliant Blue stain. **(B)** Western blot with Skd3 antibody (Abcam ab76179) showing immunoreactivity of a singular band of purified $_{MPP}$Skd3. **(C)** Western blot with Skd3 antibody (Abcam ab87253) showing immunoreactivity of a singular band of purified $_{MPP}$Skd3. **(D)** Western blot with Skd3 antibody (Proteintech #5743-1-AP) showing immunoreactivity of a singular band of purified $_{MPP}$Skd3.

bioRxiv preprint doi: https://doi.org/10.1101/2020.01.17.911016; this version posted January 18, 2020. The copyright holder for this preprint (which was not certified by peer review) is the author/funder. All rights reserved. No reuse allowed without permission.

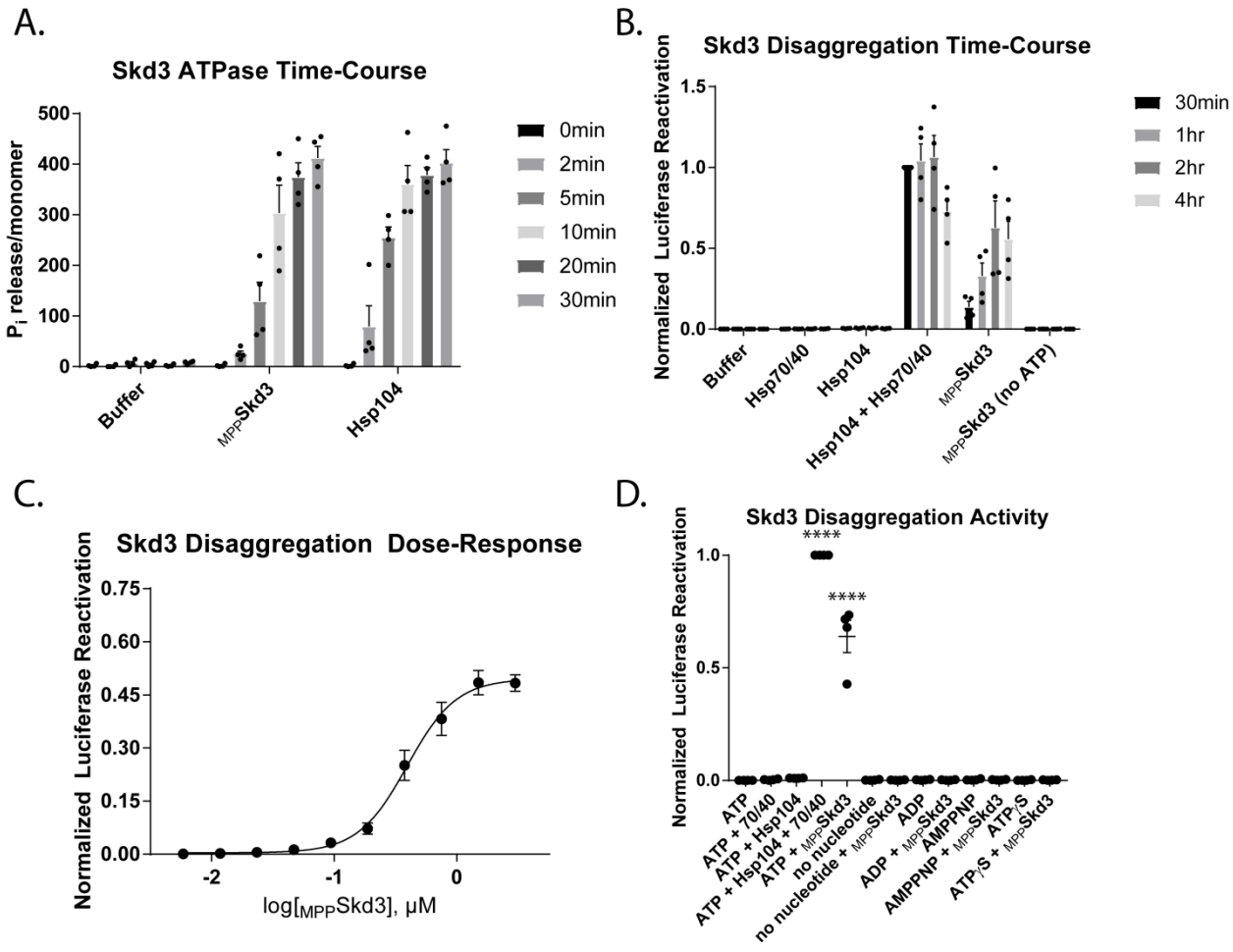

Figure S4. Skd3 is a protein disaggregase. (A) ATPase assay time course showing that $_{MPP}$Skd3 ATPase activity is approximately linear over the first five minutes of the assay. (N=4, bars show mean ± SEM). **(B)** Luciferase disaggregation/reactivation activity time course showing that $_{MPP}$Skd3 disaggregates more luciferase over time (N=4, bars show mean ± SEM). **(C)** Luciferase disaggregation/reactivation assay showing dose-response relationship between $_{MPP}$Skd3 concentration and luciferase reactivation (N=4, dots show mean ± SEM, EC_{50}=0.394µM). **(D)** Luciferase disaggregation/reactivation assay showing $_{MPP}$Skd3 disaggregase activity in the presence of different nucleotides. Results show that $_{MPP}$Skd3 can disaggregate luciferase in the presence of ATP, but not in the absence of ATP, in the presence of ADP, or in the presence of ATP analogues ATPγS (slowly hydrolyzable) or AMP-PNP (non-hydrolyzable). Luciferase assay incubated for 30 min and no ATP regeneration system was used (N=4, individual data points shown as dots, bars show mean ± SEM, **** $p<0.0001$).

bioRxiv preprint doi: https://doi.org/10.1101/2020.01.17.911016; this version posted January 18, 2020. The copyright holder for this preprint (which was not certified by peer review) is the author/funder. All rights reserved. No reuse allowed without permission.

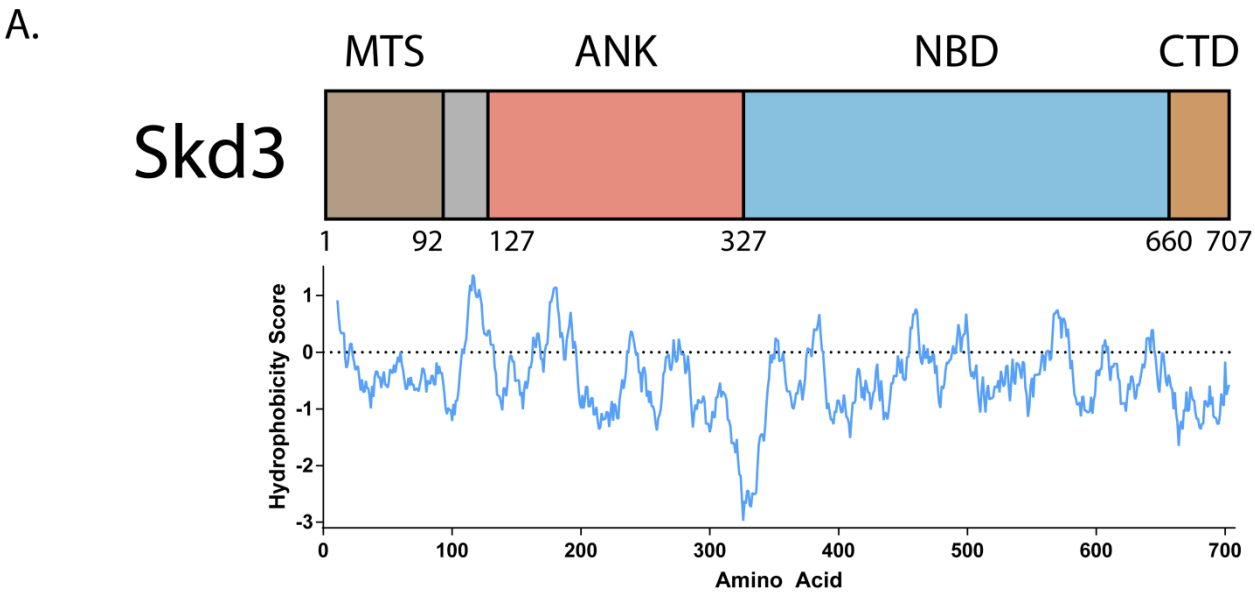

Figure S5. The auto-inhibitory domain of Skd3 is hydrophobic. (A) Kyte-Doolittle hydrophobicity score was calculated for Skd3 using the ExPASy web server(Kyte and Doolittle, 1982; Wilkins et al., 1999). A positive hydrophobicity score indicates highly hydrophobic regions. Analysis shows a spike in hydrophobicity corresponding to the inhibitory domain of Skd3.

bioRxiv preprint doi: https://doi.org/10.1101/2020.01.17.911016; this version posted January 18, 2020. The copyright holder for this preprint (which was not certified by peer review) is the author/funder. All rights reserved. No reuse allowed without permission.

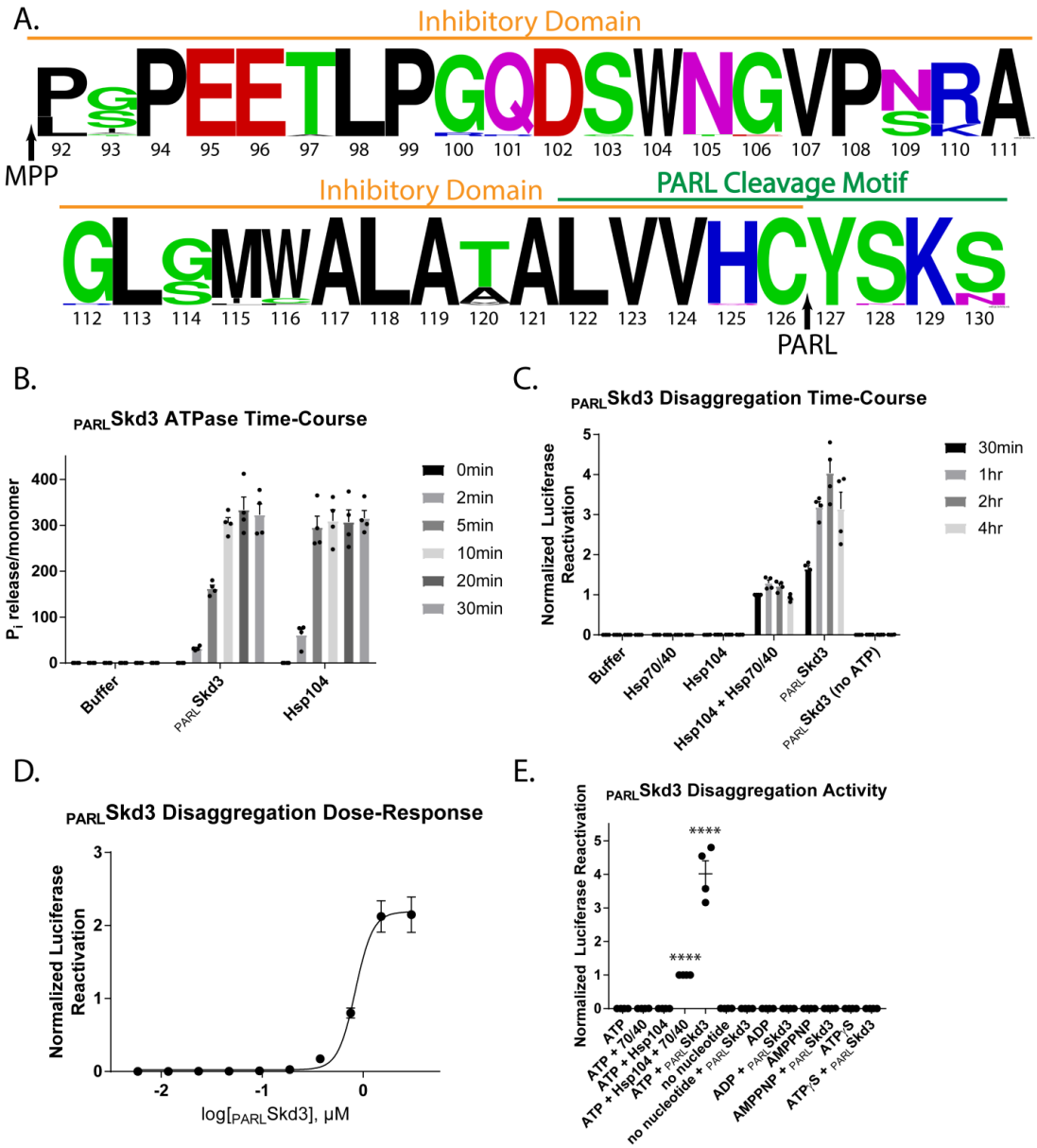

Figure S6. PARL cleavage of Skd3 enhances Skd3 disaggregase activity. (A) Sequence logo depicting the conservation of the auto-inhibitory domain (orange) and PARL-cleavage motif (green) of Skd3. Arrows indicate MPP and PARL cleavage sites. Logo shows a high level of homology suggesting conserved importance. Sequence Logo was built with WebLogo using Skd3 protein sequence from 42 different mammalian species. **(B)** ATPase assay time course showing that PARLSkd3 ATPase activity is approximately linear over the first five minutes of the assay (N=4, bars show mean ± SEM). **(C)** Luciferase disaggregation/reactivation activity time course showing that PARLSkd3 disaggregates more luciferase over time (N=4, bars show mean ± SEM). **(D)** Luciferase disaggregation/reactivation assay showing dose-response relationship between PARLSkd3 concentration and luciferase reactivation (N=4, dots show mean ± SEM, EC_{50}=0.836µM). **(E)** Luciferase disaggregation/reactivation assay showing PARLSkd3 disaggregation activity in the presence of different nucleotides. Results show that PARLSkd3 can disaggregate luciferase in the presence of ATP, but not in the absence of ATP, in the presence of ADP, or in the presence of non-hydrolyzable ATP analogues ATPγS or AMP-PNP. Luciferase assay incubated for 30 min and no ATP regeneration system was used. (N=4, individual data points shown as dots, bars show mean ± SEM, **** $p<0.0001$).

bioRxiv preprint doi: https://doi.org/10.1101/2020.01.17.911016; this version posted January 18, 2020. The copyright holder for this preprint (which was not certified by peer review) is the author/funder. All rights reserved. No reuse allowed without permission.

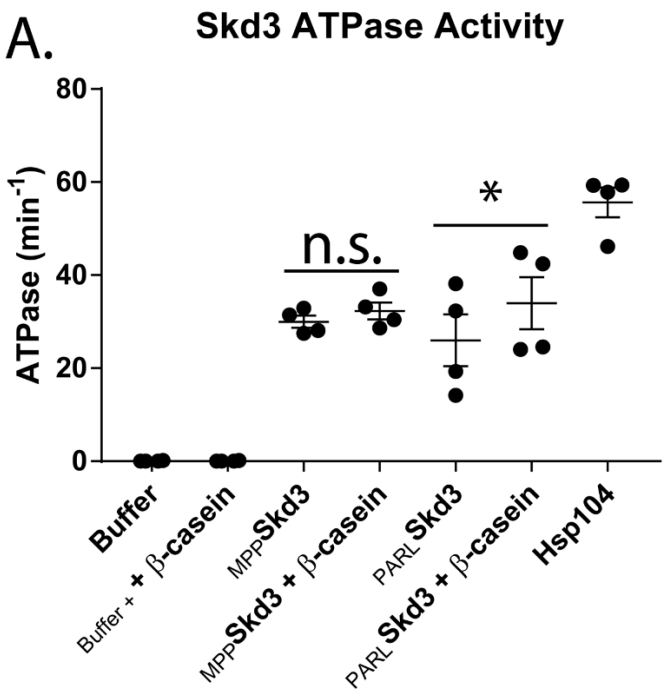

Figure S7. $_{PARL}$Skd3, but not $_{MPP}$Skd3, ATPase activity is stimulated by a model substrate. (A) ATPase assay showing that $_{PARL}$Skd3 but not $_{MPP}$Skd3 is stimulated by the model substrate β-casein. ATPase activity with substrate was compared to controls without substrate using a two-tailed, unpaired t-test. (N=4, individual data points shown as dots, bars show mean ± SEM, * $p<0.05$).

bioRxiv preprint doi: https://doi.org/10.1101/2020.01.17.911016; this version posted January 18, 2020. The copyright holder for this preprint (which was not certified by peer review) is the author/funder. All rights reserved. No reuse allowed without permission.

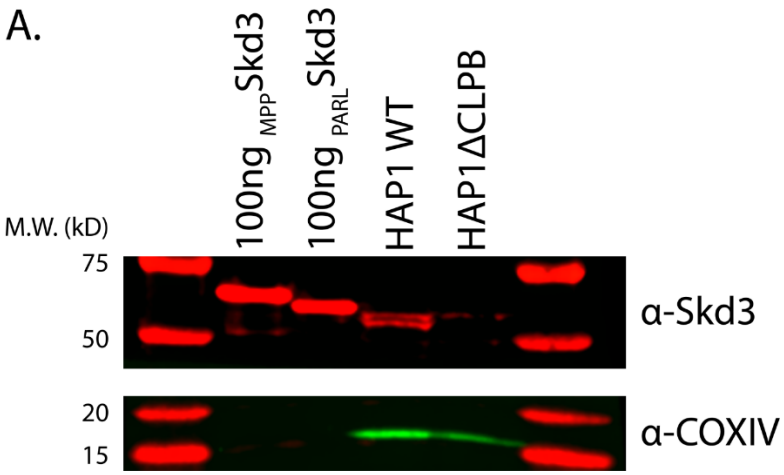

Figure S8. Verification of Skd3 knockout in HAP1 cells. **(A)** Representative western blot of HAP1 cells showing knockout of Skd3. First and second lane show 100ng load of recombinant $_{MPP}$Skd3 and $_{PARL}$Skd3. Anti-Skd3 (Abcam CAT# ab235349) and anti-COXIV (Abcam CAT# ab14744) antibodies were used.

bioRxiv preprint doi: https://doi.org/10.1101/2020.01.17.911016; this version posted January 18, 2020. The copyright holder for this preprint (which was not certified by peer review) is the author/funder. All rights reserved. No reuse allowed without permission.

A.

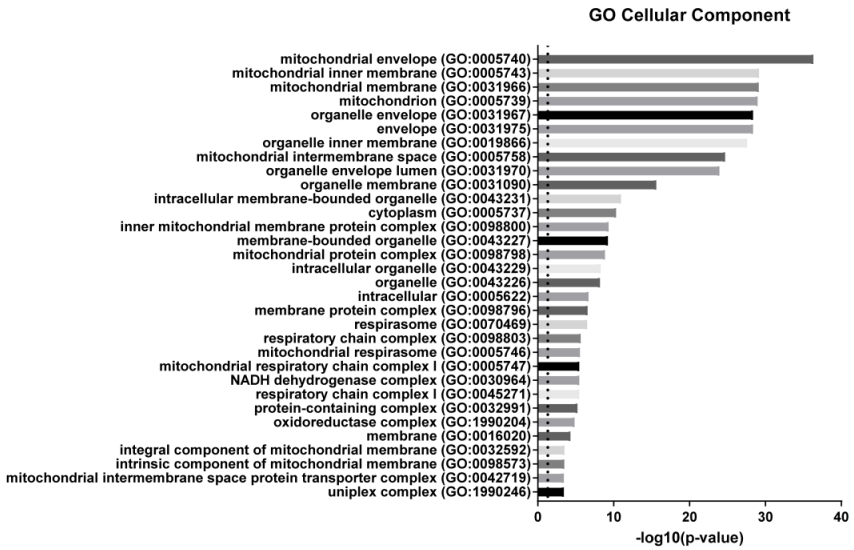

B.

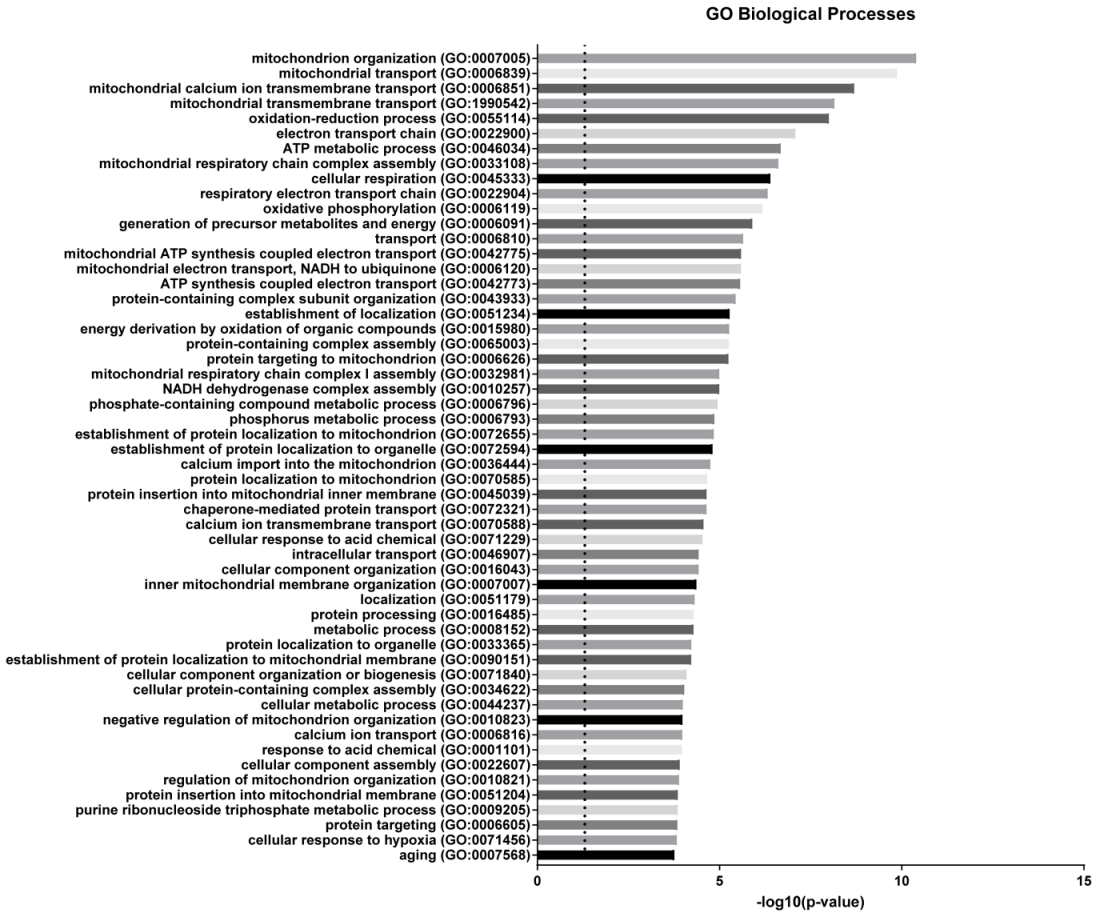

Figure S9. Skd3 deletion increases insolubility of mitochondrial inner membrane and intermembrane space proteins. (A) Terms for GO cellular component associated with the enriched proteins in the Skd3 knockout pellet. Dashed line shows p = 0.05 (p<0.05). **(B)** Full list of terms for GO biological processes associated with the enriched proteins in the Skd3 knockout pellet. Dashed line shows p = 0.05 (p<0.05).

bioRxiv preprint doi: https://doi.org/10.1101/2020.01.17.911016; this version posted January 18, 2020. The copyright holder for this preprint (which was not certified by peer review) is the author/funder. All rights reserved. No reuse allowed without permission.

A.

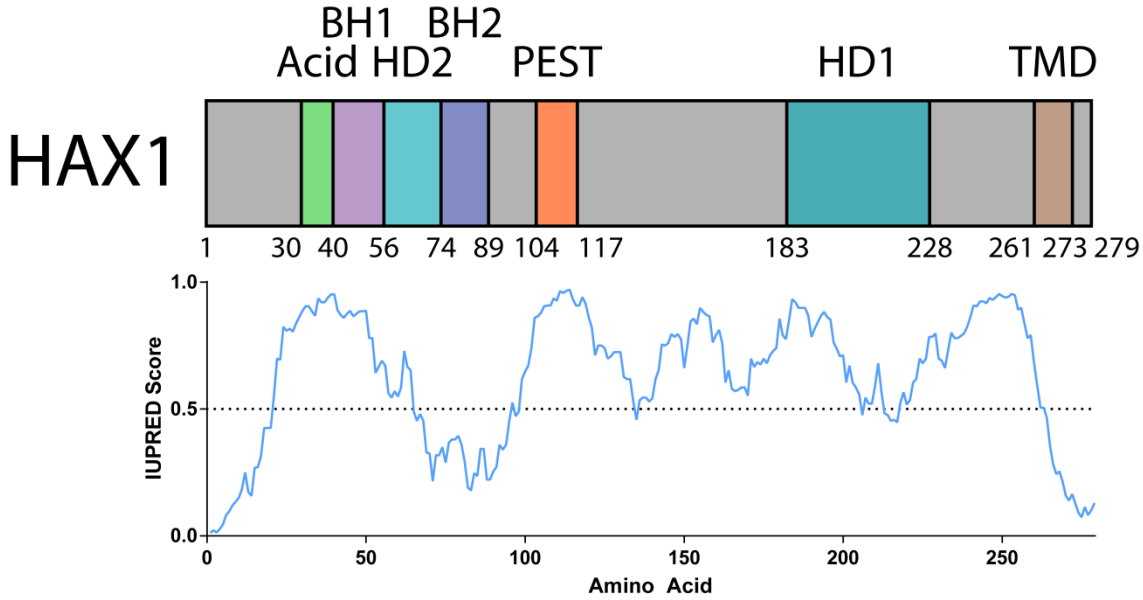

Figure S10. HAX1 is a highly disordered protein. (A) Domain map of HAX1 with IUPRED disorder prediction score plotted underneath. IUPRED scores higher than 0.5 predict disorder. Analysis suggests that HAX1 is a highly disordered protein. Acidic domain labeled in green, BH1 and BH2 domains labeled in purple, HD1 and HD2 domains labeled in blue, PEST domain labeled in orange, and transmembrane domain (TMD) labeled in tan.

Table S1: Proteins enriched in HAP1 *ΔCLPB* cell pellet. Proteins from mass spectrometry data in Figure 7b highlighted in red that have >2.0 fold change increase in the *ΔCLPB* cell pellet compared to WT and a p-value of <0.05.

Table S2: Proteins enriched in HAP1 WT cell pellet. Proteins from mass spectrometry data in Figure 7b highlighted in green that have >2.0 fold change increase in the WT cell pellet compared to *ΔCLPB* and a p-value of <0.05.